Noname manuscript No.
(will be inserted by the editor)

Connecting Mem-Models with Classical Theories

Jin-Song Pei · François Gay-Balmaz · Darby J. Luscher · James L. Beck · Michael D. Todd · Joseph P. Wright · Yu Qiao · Marco B. Quadrelli · Chuck R. Farrar · Nicholas A. J. Lieven

Received: date / Accepted: date

Abstract

A family of mem-models, including the mem-dashpots, mem-springs, and most recently, mem-inerters, is emerging as a new and powerful way of capturing complex nonlinear behaviors of materials and systems under various types of dynamic loads involving different frequency, amplitude, and loading histories (e.g., hysteresis). Under the framework of nonlinear state-space representation and hybrid dynamical systems, mem-springs may be formulated to effectively represent an inherent degradation of material state. It is shown in this study, for the first time, how the absement (time integral of strain /displacement), a signature state variable for a mem-spring, can be connected with the damage variable, a key quantity in continuum damage mechanics (CDM). The generalized momentum (time integral of stress), on the other hand, is shown to be efficient in modeling strain ratcheting via the concept of mem-dashpot. It is also shown in this study, for the first time, how two formulations of the memcapacitive system models (for mem-springs) are special cases of the Preisach model.

Keywords: Mem-models, absement, generalized momentum, nonlinear state-space representation, hybrid dynamical system, continuum damage mechanics, damage variable, strain ratcheting, Wiechert model, classical Preisach model

Jin-Song Pei (✉)
School of Civil Engineering and Environmental Science
University of Oklahoma
Norman, Oklahoma 73019-1024
Tel.: +1-405-325-4272
Fax: +1-405-325-4217
E-mail: jspei@ou.edu

François Gay-Balmaz
CNRS LMD
Ecole Normale Supérieure de Paris
24 Rue Lhomond
75005 Paris, France

Darby J. Luscher and Chuck R. Farrar
Los Alamos National Laboratory
Los Alamos, NM 87545

James L. Beck
California Institute of Technology
Mail Code 9-94
Pasadena. CA 91125

Michael D. Todd and Yu Qiao
Department of Structural Engineering
University of California, San Diego
9500 Gilman Drive, Mail Code 0085
La Jolla, CA 92093

Joseph P. Wright
Division of Applied Science
Weidlinger Associates Inc.
New York, NY 10005

Marco B. Quadrelli
Jet Propulsion Laboratory
California Institute of Technology
Pasadena, CA 91109

Nicholas A. J. Lieven
University of Bristol
Bristol BS8 1TH U.K.

1 INTRODUCTION

Classical theories treating viscoelasticity, viscoplasticity, damage, and hysteresis modeling constantly call for a continuous development to accommodate the requirements/opportunities of never-ending real-world challenges, active engineering innovations, and greatly enhanced information technology capabilities. In this study, classical theories are identified and connected with an emerging new family of models called "mem-models" that originated from

bond graph theory, and has evolved to underpin hybrid dynamical system theory. Figs. 1 to 3 are snapshots demonstrating modeling capabilities of mem-models that complement those of the existing models and are achieved in a computationally efficient manner. For each of these sets of responses, we will show how existing concepts from different fields can be connected to mem-models. These new connections will enrich mem-modeling development and application and provoke a new appreciation of classical theories in damage mechanics and hysteresis modeling. Specific definitions of mem-dashpots and mem-springs will be introduced as we proceed as a partial overview of mem-models; see Pei et al (2015) for background material and general definitions. The relevant classical theories in damage mechanics and hysteresis modeling will also be briefly reviewed for clarity.

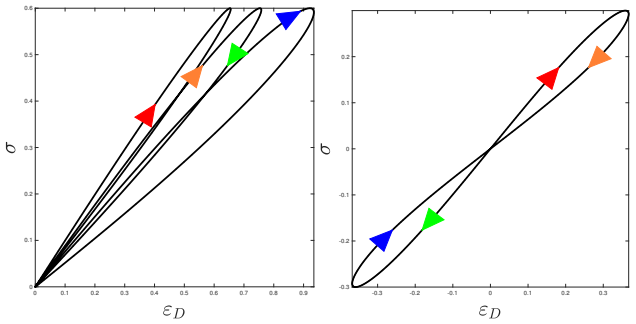

(a) cycle-to-cycle recovery introduced by using absement-based mem-spring modeling

(b) dissipative and symmetrical responses in two directions enabled by mem-spring modeling

Fig. 1: Modeling capabilities of a specific 1-D damage model in CDM (a mem-spring model in fact) after being improved by using the hybrid dynamical system view that is introduced to mem-spring modeling following Pei (2018). The model will be given in conjunction with Fig. 8; the inputs are $\sigma(t) = 0.3(1 - \cos(6t))$ and $\sigma(t) = 0.3\sin(2t)$ for (a) and (b), respectively. Arrowheads in red, orange, green and blue (in this order) are used for the orientation of the loops herein

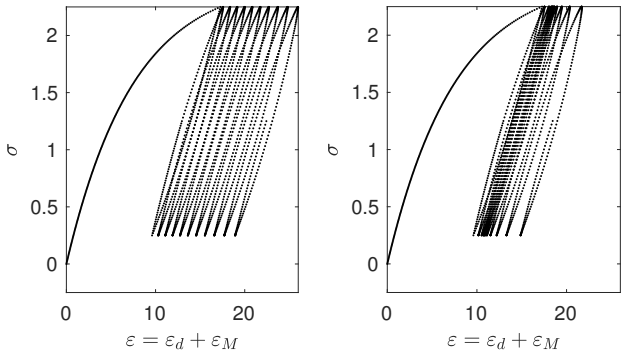

(a) softening memristor

(b) hardening-softening memristor

Fig. 2: Fatigue softening and fatigue hardening-softening strain ratcheting responses efficiently simulated by using generalized momentum-based mem-dashpot modeling. The models for the ratcheting strain ε_d will be presented in conjunction with Fig. 11 (b) and (c)

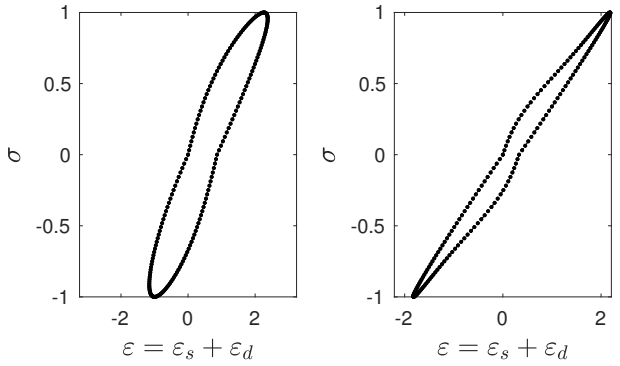

(a) An assembly whose parameters follow Table 4 Case 1

(b) An assembly whose parameters follow Table 4 Case 2

Fig. 3: Nonlinear periodic responses to sinusoidal input enabled by assemblies of a mem-spring and mem-dashpot that have the same creep response to two different Wiechert models. These are snapshots extracted and rescaled from Fig. 18

1.1 Motivation for Mem-Modeling

Complex nonlinear dynamic behaviors/responses have been studied for the purposes of modeling, simulation, monitoring, and control. Linear and nonlinear state-space representations are attractive given that they bridge the gap between data and model, and facilitate system identification and control in a reduced-order modeling fashion. Nonetheless, the choice of state variables has been (and is) a challenge. Kalman (1967) pp. 135 states: "the state is the least amount of information we need about past inputs to determine the output resulting from any future input". Willems (1972), pp. 325 states: "It is, however, impossible to deduce a priori, in physical terms what will be the state. This indeed, is a very difficult problem even for relatively simple systems, and it appears to be the cause for much of the reluctance of introducing this concept in physics". Analogously, within the field of continuum constitutive theory, the thermodynamic state of a system is a full description of its instantaneous condition which is identified by a set of state variables. The set of state variables represent the minimum information to define all thermodynamic properties of the system.

The same may be said about mem-spring models that belong to the mem-model class. Not only is the choice of state variables unclear, but also the required functional forms defining both the state evolution and input-output mappings are not precisely defined. Material stress-strain behaviors and system load-displacement responses characterized by the "origin-crossing" input-output feature (meaning that the

input and output become zero simultaneously) under repetitive loading and unloading conditions may be modeled efficiently by mem-spring models.

Mem-springs are from a new family of state-space hysteresis models called "mem-models" introduced to engineering mechanics in Pei et al (2015, 2017); Pei (2018); Pei et al (2020a,b); Wagg and Pei (2020). They are based on a suite of new concepts for the memristor, memcapacitor, and meminductor developed in electrical engineering originated in Chua (1971), catching attention since Strukov et al (2008) and being generalized in Di Ventra et al (2009). The publications on mem-dashpots, mem-springs, and mem-inerters followed the lead of Oster and Auslander (1973); Jeltsema (2012) when the memristor was first introduced to engineering mechanics.

Unlike mem-dashpot models, mem-spring models are fundamentally new, and as such **there are no well-established existing examples for these models. Devising a mem-spring model by defining the required functional forms does not have general guidelines, which are the focus of our pursuit.** To construct mem-models, we have tried using experimental data and secant quantities (Pei et al (2020a)). This is one way of obtaining mem-spring models, which may work. However, it neither helps to explain why or when it works, nor to predict situations when it does not work. Another way we have tried is to overcome the limitation of mem-spring models that are revealed by the phenomenon to be modeled and then supplement the models with other theories/techniques, e.g., modify the original definitions of the mem-models by following hybrid dynamical system theory (Pei (2018)). In this study, we try a different approach. We start with some existing theories that have no apparent connections to mem-models and arrive at some specific forms of mem-spring models. This is a rigorous but limited way of constructing mem-models; however, the connections with established physical models provide potentially better insights. This path was previously exercised in Pei (2018), which examined creep and relaxation responses in viscoelasticity.

We start with a simple 1-D damage model in CDM and show that it is actually a mem-spring model. In addition, we explain what absement could mean and also what the CDM damage variable signifies physically from this mem-model viewpoint. We then go further to improve a subset of the 1-D damage models by using techniques developed for mem-springs. We also examine a mem-spring model by using the definition of hyperelasticity, e.g., Houlsby and Puzrin (2007), which is akin to augmenting the state description of the material with a set of internal state variables, the so-called internal state variable theory (ISV) of both kinematic and kinetic types as enabled by the mem-models.

Next, we take the simplest mem-dashpot model called a mechanical memristor to show its usefulness in modeling ratcheting strain and its potential in viscoplasticity. We then turn to assemblies of one mem-spring and one mem-dashpot. In a parametric study, we calibrate such a mem-model assembly with a two-arm Wiechert model (Roylance (2001)) in terms of one particular creep response, after which we compare the two different models for both sinusoidal and consecutive positive loading responses. The Wiechert model is a popular choice in viscoelasticity, making such a connection useful.

Then, we examine a subset of the classical Preisach models (Preisach (1935); Krasnosel'skii and Pokrovskii (1989); Mayergoyz (2003)) that can be represented by mem-models. We show, step by step, how an order-1 Preisach model can be written as a mem-spring model by assigning a proper state variable under the state-space representation. We arrive at two forms of mem-models, one being exact and the other approximate. Both of them are loading rate independent. As the order of the Preisach response increases, we need more state variables for the mem-models. This is a constructive approach for devising mem-spring model architectures.

Finally, we examine the generalized Duhem model (Padthe et al (2008)) and point out its relationship with the mem-models.

1.2 Motivation from Continuum Damage Mechanics and Rheological Models

Eq. (1.6) in Kachanov (1986) gives the elastic strain of a damaged material as $\varepsilon = \frac{1}{E}\frac{\sigma}{\Phi}$, where Φ is called "continuity", a positive monotonically decreasing function of time, i.e., $\dot{\Phi} < 0$ and $1 \geq \Phi \geq 0$. A simple form of the kinetic equation in the case of uniaxial tension is given in Eq. (1.8) in Kachanov (1986) as $\frac{d\Phi}{dt} = -A\left(\frac{\sigma}{\Phi}\right)^n$. Lemaitre (1996) states: "... About fifteen years later $D = (1 - \Phi)$ received the status of an internal state variable in the thermodynamical sense: $0 \leq D \leq 1$ (0 for the undamaged state and 1 for failure)", where D is ξ in this paper. The damage variable is an abstract concept as it was created for modeling purpose. This concept is typically introduced to represent a phenomenological degradation in material response, often without a precise physical definition.

An internal state variable is often not directly measurable making it harder to comprehend. In this study, we use the mem-spring theory to quantitatively express the damage variable by using absement, a concept essential in mem-spring theory. When the exponent $n = 1$, the damage variable depends on the absement only. When $n \neq 1$, the damage variable rate depends on the absement rate. Even though absement is not often used, it indeed is a kinematic quantity that could be obtained from time integral of strain. Thus, **we demystify the concept of the damage variable**. We make this internal state variable more observable.

Damage functions in CDM are nonlinear and generally irreversible. Mem-models are also fundamentally nonlinear, rate-dependent (but can be made rate-independent), and can be made hysteretic. This versatility suggests to us that mem-models may allow more versatile damage mechanisms, and overcome some current limitations of CDM, e.g., nonlinear accumulation of damage and the effect of mean stress in fatigue (see page 98 in Lemaitre (1996)); see Fig. 2. Mem-models offer an alternative framework for CDM damage functions to improve, generalize, and evolve in modeling both elasticity and plasticity with history dependency. The hybrid dynamical system framework (mentioned in Fig. 1), secant modulus-based identification, and dual input-output pairs are among new techniques/ways of thinking that mem-models can bring to "classical" CDM as described in Kachanov (1986); Lemaitre (1996).

Networks of mechanical elements (spring, dashpot, etc.) have been used as rheological models, e.g., in viscoelasticity, viscoplasticity and even extended to material damage (e.g., Houlsby and Puzrin (2007)). As a source of nonlinearity and degradation, damage variables are treated as internal state variables separately from other state variables that are kinematic quantities. In contrast, mem-dampers and mem-springs individually are more powerful than their linear counterparts in modeling (Pei et al (2020a)). This hints at a simpler network involving fewer parameters to be identified when introducing mem-models in a network. See Fig. 3 for richer responses that the smallest mem-model assembly can bring about with the same number of parameters as its linear counterpart (a Wiechert model in that case). Mathematically, mem-dashpots and mem-springs can degenerate into their linear counterparts.

1.3 Motivation from Hysteresis Modeling

Hysteresis modeling has a long and still active history, see Morris (2011) for a review. Herein, we examine whether mem-models can be useful for hysteresis modeling. There are two types of hysteresis models: physics-based and phenomenological. The latter is excellent for minor loop prediction. There are several sub-types under phenomenological models, for example, differential equation-based, hysteresis operator-based, summation of elements-based. See Table 1. Mem-models can be classified as belonging to the first two sub-types: differential-equation-based models (e.g., Pei et al (2017)) and as shown in this study, classical Preisach models (which are hysteresis operator-based).

Not to be exhaustive, Table 2 lists some hysteresis operator-based models, which are all classical Preisach models. In particular, DEM, extended Masing, and Maxwell slip models are equivalent, being a subset of the classical Preisach model. As reviewed in Pei and Beck (2020), this understanding comes from model equivalency, which was initiated in Jayakumar (1987); Jayakumar and Beck (1988); Beck and Jayakumar (1996), peaked in Lubarda et al (1993), and promoted in Segalman and Starr (2004, 2008); Royston (2008). We will show that mem-spring models can be formulated into a subset of the classical Preisach models.

Table 1 uses four popular model classes for hysteresis to examine the three sub-types under phenomenological representation, where the importance of nonlinear state space modeling can be seen; mem-models are naturally nonlinear state space models.

Gorbet et al (1998) invokes the classical state-space representation of Willems (1972) to show that the classical Preisach model falls within the standard dynamical system framework, legitimizing the representation using state space. Since extended Masing and DEM are equivalent and are a subset of the classical Preisach model, they follow suit. We highlight the necessity of using differential algebraic equation (DAE) and hybrid system, as elaborated and demonstrated in Pei and Beck (2020) to implement the hysteresis rules defining the extended Masing model. Note that the Bouc-Wen model is not a subset of classical Preisach models (Pei and Beck (2020)). The use of a summation of elements starts with the well-known Kelvin and Maxwell models assembled from spring and dashpot elements. DEM and extended Masing have been presented by a summation of stops or plays (Iwan (1966, 1967); Jayakumar (1987); Jayakumar and Beck (1988); Beck and Jayakumar (1996)), while the classical Preisach model is a summation of relay hystrons (Krasnosel'skii and Pokrovskii (1989); Mayergoyz (2003)).

1.4 Contributions and Structure of this Paper

An overarching goal of this work is to further the understanding of mem-modeling by building connections to classical theories, showing how mem-models either complement or improve these existing theories, and reciprocally, how the latter can inspire new development in mem-modeling.

In Section 2, we identify an existing simple 1-D CDM model as a mem-spring model so that we can learn from the choice of functional forms that mem-spring modeling has been lacking. We quantify the relationship between the damage variable in this CDM model and the state variable called absement in mem-modeling (time integral of strain). For a subset of this 1-D CDM model with $n = 1$, we improve it by using mem-spring modeling techniques to produce new or more desirable responses. We outline what a 3-D mem-spring model would look like.

In Section 3, we point out the usefulness of another state variable called generalized momentum in mem-modeling (time integral of stress), in the context of modeling 1-D ratcheting strain. We develop a mechanical memristor-based

Table 1: Three sub-types for phenomenological hysteresis models. †with a necessity of involving differential algebraic equation (DAE) and hybrid system

Model Class	**Sub-Type of Phenomenological Representation**		
	Nonlinear State-Space	Classical Preisach	Summation of Elements
Bouc-Wen	Yes	No	No
Classical Preisach	Yes in Principle † (Gorbet et al (1998); Pei et al (2017) and this study)	Yes	Yes (Krasnosel'skii and Pokrovskii (1989); Mayergoyz (2003))
Extended Masing	Yes † (Jayakumar (1987); Jayakumar and Beck (1988); Beck and Jayakumar (1996); Pei and Beck (2020))	Yes (Lubarda et al (1993))	Yes (Jayakumar (1987); Jayakumar and Beck (1988); Beck and Jayakumar (1996))
DEM	Yes in Principle †	Yes (Lubarda et al (1993))	Yes Iwan (1966, 1967)

Table 2: Some hysteresis operator-based models

	Model Name	Selected Reference
1	Classical Preisach models	Preisach (1935); Krasnosel'skii and Pokrovskii (1989); Mayergoyz (2003)
2	Play & stop	Visintin (1994)
3	Generalized play & generalized stop	Krasnosel'skii and Pokrovskii (1989); Visintin (1994)
4	Prandtl-Ishlinskii model	Visintin (1994)
5	Krasnosel'skii-Pokrovskii model	Krasnosel'skii and Pokrovskii (1989)
6	Maxwell slip model (Maxwell resistive capacitive model)	Goldfarb and Celanovic (1996)
7	Distributed-element model (DEM)	Iwan (1966, 1967)
8	Extended Masing model	Masing (1926); Fan (1968); Pyke (1979); Jayakumar (1987); Jayakumar and Beck (1988); Beck and Jayakumar (1996)

model for this application. We compare a two-arm Wiechert model with the smallest assembly of a mem-spring and a mem-dashpot to exploit the richness of the mem-models' dynamic responses, in relation to their linear counterparts.

In Section 4, we connect two forms of mem-spring models to a subset of classical Preisach models. Overall, even though we make a connection between mem-springs and the classical Preisach models, non-deteriorating hysteresis model, we highlight the inherent "damaging", or "degrading" properties that are built into the mem-models, which we exploit for CDM and viscoelasticity.

2 MEM-SPRING MODELS AND CONTINUUM DAMAGE MECHANICS

There is a connection between mem-spring models and the damage function in continuum damage mechanics. Understanding and exploiting this connection will help advance both mem-models and continuum damage mechanics.

2.1 Relationship of 1-D CDM Damage Model and Memcapacitive System Model

An effort-controlled (i.e., force/stress-controlled) memcapacitive system model can be expressed as follows:

$$\text{state equations:} \quad \dot{\mathbf{y}}(t) = \mathbf{f}\left(\mathbf{y}(t), r(t), t\right) \tag{1}$$

$$\text{input-output equation:} \quad x(t) = C\left(\mathbf{y}(t), r(t), t\right) r(t), \tag{2}$$

where $\mathbf{y}(t)$ is a state vector, $r(t)$ is the restoring force/stress, and $x(t)$ is the displacement/strain. In this constitutive relation, the input is $r(t)$, while the output is $x(t)$. In general, the secant compliance function, C, depends on the states and input. To arrive at specific functional forms for this model, we examine a specific CDM model for hints.

Isolating the 1-D continuum damage mechanics (CDM) model from Kachanov (1986) and casting it into the format for an effort-controlled memcapacitive system model, we have the following:

$$\text{state equation:} \quad \dot{\xi} = A\left(\frac{\sigma}{1-\xi}\right)^n \tag{3}$$

$$\text{input-output equation:} \quad \varepsilon_D = \frac{1}{E(1-\xi)}\sigma, \tag{4}$$

where $A > 0$ and $n \geq 1$ are material properties. In this constitutive relation, the input $r(t)$ is the stress $\sigma(t)$, while the output $x(t)$ is the "elastic-damage" strain $\varepsilon_D(t)$. The scalar state variable $y(t)$ in Eq. (1) is the damage variable $\xi(t)$,

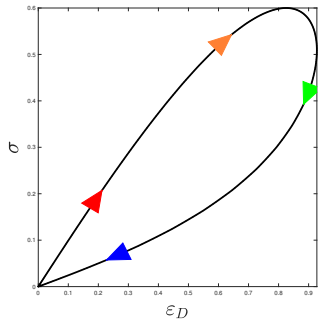

(a) $A = 0.5$, $n = 1$, and $E = 1$ with $\sigma(t) = 0.3(1 - \cos(2t))$

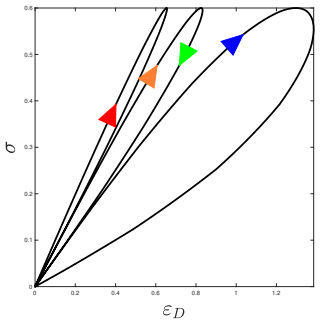

(b) $A = 0.5$, $n = 1$, and $E = 1$ with $\sigma(t) = 0.3(1 - \cos(6t))$

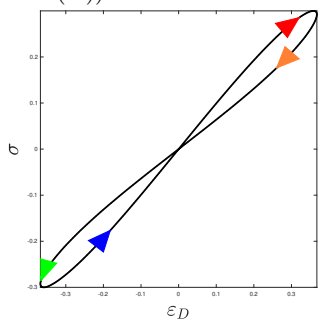

(c) $A = 1$, $n = 1$, and $E = 1$ with $\sigma(t) = 0.3\sin(2t)$

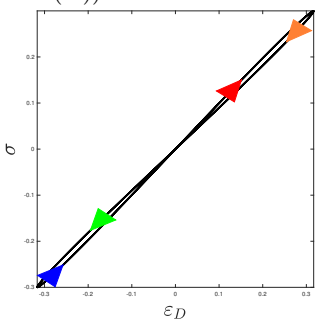

(d) $A = 1$, $n = 1$, and $E = 1$ with $\sigma(t) = 0.3\sin(6t)$

Fig. 4: Two different 1-D CDM damage models with $n = 1$ subject to a total of four specific stress inputs. Note that (b) does not take into consideration partial recovery from cycle to cycle. (c) and (d) are not physically meaningful. Improved models are shown in Fig. 1 with details to be given in Section 2.3

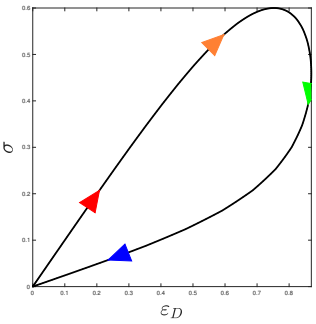

(a) $A = 0.775$, $n = 2$, and $E = 1$ with $\sigma(t) = 0.3(1 - \cos(2t))$

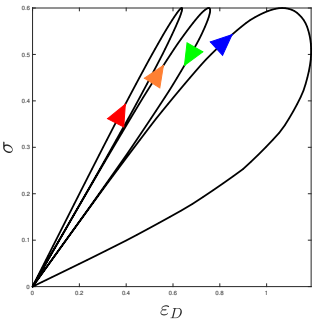

(b) $A = 0.775$, $n = 2$, and $E = 1$ with $\sigma(t) = 0.3(1 - \cos(6t))$

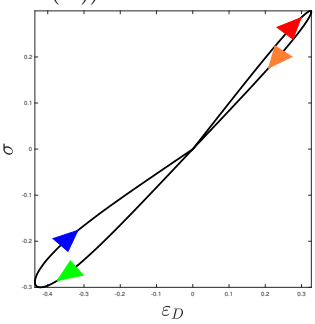

(c) $A = 2$, $n = 2$, and $E = 1$ with $\sigma(t) = 0.3\sin(2t)$

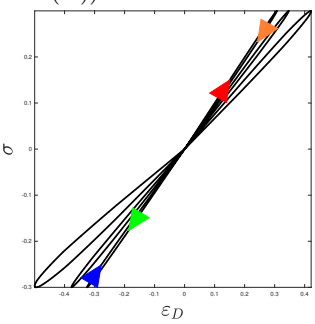

(d) $A = 2$, $n = 2$, and $E = 1$ with $\sigma(t) = 0.3\sin(6t)$

Fig. 5: Two different 1-D CDM damage models with $n = 2$ subject to a total of four specific stress inputs. Note that (b) does not take into consideration partial recovery from cycle to cycle. (c) and (d) are physically meaningful, however antisymmetric patterns may be desired from time to time. Improved models are shown in Fig. 1 with details to be given in Section 2.3

and E is the initial modulus of elasticity. In a continuum thermodynamics setting of CDM, Eq. (4) would be identified as the "state relation" and Eq. (3) as the "kinetics." It is important to note that ε_D is the total damaged and elastic strain. This is not reversible nonlinear elasticity; rather the process is irreversible and dissipative but the strain can all be recovered by removing the stress; i.e., $\sigma \to 0$ and $\varepsilon_D \to 0$ simultaneously, conforming to the so-called zero-crossing property. Figs. 4 and 5 give two numerical examples with $n = 1$ and $n = 2$, respectively; the issues specified in the figure captions in these two examples will be addressed later. Eq. (3) does not guarantee $0 \leq \xi \leq 1$, which is needed in Eq. (4); See Eq (5). The simulation must be terminated when ξ reaches 1 as typified in Fig. 6.

$$\xi(t) = 1 - \left[1 - (n+1)A \int_0^t \sigma(\tau)^n d\tau\right]^{\frac{1}{n+1}} \tag{5}$$

It can be seen that the **1-D CDM damage model is a special time-invariant effort-controlled memcapacitive system model with the single state variable** ξ. In this model, C in Eq. (2) does not depend on time or the input $r(t)$. This should not come as a surprise since CDM is an internal state variable (ISV)-based formulation; our interest is

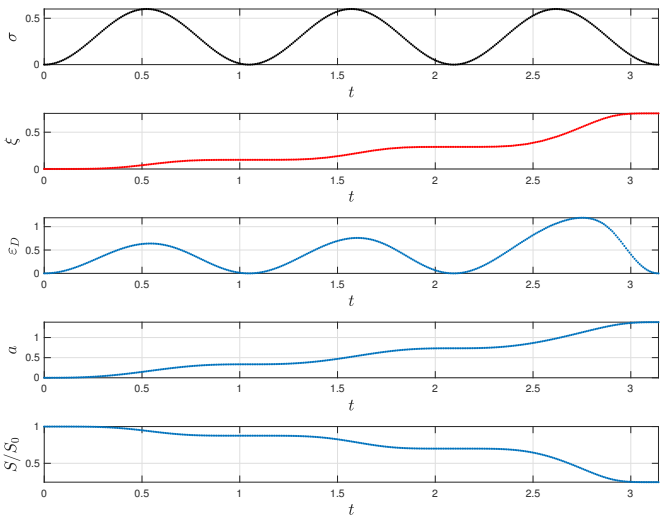

Fig. 6: A typical set of time histories, which matches Fig. 5(b) highlighting the need for $0 \leq \xi \leq 1$

whether mem-models can provide a broader framework for CDM.

2.2 Relationship between 1-D CDM Damage Variable and Absement

Equations (3) and (4) can be rewritten as a single equation by eliminating σ:

$$\frac{\dot{\xi}}{A} \;=\; (E\varepsilon_D)^n \tag{6}$$

Based on the definition of absement $a(t)$, we have:

$$\dot{a} \;=\; \varepsilon_D \tag{7}$$

Substituting Eq. (7) into Eq. (6), we have the following:

$$\dot{\xi}(t) = AE^n \dot{a}(t)^n \tag{8}$$

$$\xi(t) = AE^n \int_0^t \left(\dot{a}(\tau)\right)^n d\tau \;\text{ assuming } \xi(0) = 0, \tag{9}$$

where Eq. (8) is in a differential form, while Eq. (9) is in an integral form. Conversely, we have:

$$\dot{a}(t) = \frac{1}{E}\left(\frac{\dot{\xi}(t)}{A}\right)^{\frac{1}{n}} \tag{10}$$

$$a(t) = \frac{1}{E}\int_0^t \left(\frac{\dot{\xi}(\tau)}{A}\right)^{\frac{1}{n}} d\tau \;\text{ assuming } a(0) = 0 \tag{11}$$

For $n = 1$, $a(t) = \frac{1}{EA}\xi(t)$. Since failure of the system occurs at $\xi = 1$ in this damage mechanics model, the failure absement is $a_{\text{failure}} = \frac{1}{EA}$, giving an interpretation of the material parameter A.

These equations give a physical interpretation of the damage variable: **The absement rate and damage variable rate follow a nonlinear static one-to-one mapping. This one-to-one mapping follows a power law of n. In particular, for $n = 1$, the two rates are proportional and so are $a(t)$ and $\xi(t)$ if $\xi(0) = a(0) = 0$.**

2.3 Benefits of Absement as State Variable

A flow-controlled (i.e., displacement/strain-controlled) memcapacitive system model can be obtained analogous to Eqs. (1) and (2):

$$\text{state equations:} \quad \dot{\mathbf{y}}(t) = \mathbf{g}\left(\mathbf{y}(t), x(t), t\right) \tag{12}$$

$$\text{input-output equation:} \quad r(t) = S\left(\mathbf{y}(t), x(t), t\right) x(t) \tag{13}$$

where, as before, $\mathbf{y}(t)$ is the state vector, $r(t)$ is the restoring force/stress, and $x(t)$ is the displacement/strain. In this constitutive relation, the input is $x(t)$, while the output is $r(t)$. S is the secant stiffness function and can be seen as the general spring stiffness, a function of the states and input.

When $n = 1$ in the model in Eq. (8), the 1-D CDM damage model is equivalent to using absement a as the state (damage) variable. Furthermore, the mem-spring model is reduced to its simplest form, a mechanical memcapacitor (which is an element model), defined as follows:

$$\sigma(t) \;=\; E(1 - EAa(t))\varepsilon_D(t), \tag{14}$$

where $\dot{a}(t) = \varepsilon_D(t)$, a trivial state equation. Since $\xi(t) \leq 1$, $a(t) \leq \frac{1}{EA}$ must hold. It can be seen that the secant stiffness function is a function of a: $S(a(t)) = E(1 - EAa(t))$, which is a one-to-one mapping that can be exploited in analyzing proper data (Pei et al (2015)).

Integrating both sides of Eq. (14) with respect to time t and introducing the concept " generalized momentum" (Pei et al (2018)):

$$\dot{p}(t) = \sigma(t) \tag{15}$$

we arrive at the following one-to-one mapping from a to p that defines the mechanical memcapacitor:

$$p(t) \;=\; -\frac{E^2 A}{2}\left(a(t) - \frac{1}{EA}\right)^2 + \frac{1}{2A}, \tag{16}$$

where $a \leq \frac{1}{EA}$. Clearly, $p(t) \leq \frac{1}{2A}$. Equivalently, we have the inverse one-to-one mapping from p to a as follows:

$$a(t) \;=\; -\sqrt{\left(-\frac{2}{E^2 A}\right)\left(p(t) - \frac{1}{2A}\right)} + \frac{1}{EA} \tag{17}$$

using which we have:

$$\varepsilon_D(t) = \frac{\sigma(t)}{E\left\{1 - EA\left[\frac{1}{EA} - \sqrt{\left(-\frac{2}{E^2 A}\right)\left(p(t) - \frac{1}{2A}\right)}\right]\right\}} \tag{18}$$

which is a special case of an effort-controlled memcapacitive system model with $\dot{p}(t) = \sigma(t)$, a trivial state equation, and the secant compliance function being a function of p:

$$C(p) = \frac{1}{E\left\{1 - EA\left[\frac{1}{EA} - \sqrt{\left(-\frac{2}{E^2 A}\right)\left(p - \frac{1}{2A}\right)}\right]\right\}}$$

which is a one-to-one mapping that can also be exploited in analyzing proper data (Pei et al (2015)).

Equations (14) and (18) are equivalent, being in the flow- and effort-controlled form, respectively. This is the convenience of having an element model, which belongs to the family of higher-order elements (Chua (2003); Biolek et al (2016)) with each model governed by a one-to-one mapping of the defining kinematic and kinetic quantities. The two specific one-to-one mappings used in Fig. 4(a) and (b), and (c) and (d) are presented in Fig. 7 (a) and (b), respectively.

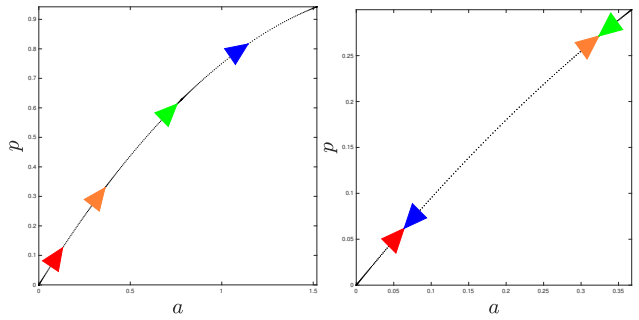

(a) for Fig. 4(a) and (b) where $A = 0.5$, $n = 1$, and $E = 1$

(b) for Fig. 4(c) and (d) where $A = 1$, $n = 1$, and $E = 1$

Fig. 7: The one-to-one mappings between $a(t)$ and $p(t)$ used in Fig. 4

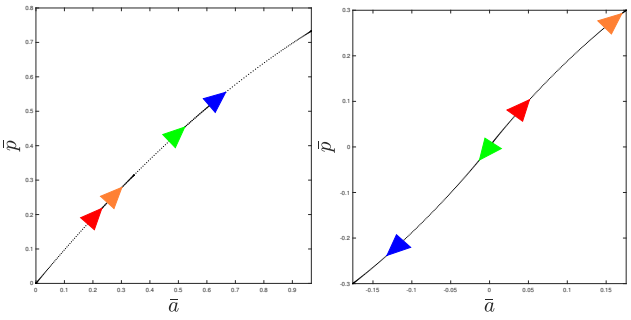

(a) for Fig. 1(a) where $A = 0.5$, $n = 1$, and $E = 1$

(b) for Fig. 1(b) where $A = 1$, $n = 1$, and $E = 1$

Fig. 8: The one-to-one mappings between $\bar{a}(t)$ and $\bar{p}(t)$ used in Fig. 1

The response presented in Fig. 4(b) does not take partial recovery from cycle to cycle into account. Following the technique and examples in Pei (2018), a one-mode hybrid system model can be adopted to improve the current model. Namely, "reset" is applied to both $a(t)$ and $p(t)$ whenever a new consecutive positive cycle starts. These reset quantities are denoted as $\bar{a}(t)$ and $\bar{p}(t)$. The one-to-one mapping between a and p still holds but in terms of $\bar{a}(t)$ and $\bar{p}(t)$; see Figs. 8(a) and 1(a) for the improved one-to-one mapping and the response, respectively.

Energy generating behavior (i.e., non-passivity) occurs in both Fig. 4(c) and (d). This is a fundamental challenge to overcome for mem-spring models as detailed in Pei et al (2015); Pei (2018). In addition to the techniques exercised there, we try the following "reset" in this study: the integrations of ε_D and σ for a and p will be reset into $\bar{a}$ and $\bar{p}$, respectively, whenever the loading changes its direction. Under each loading direction, the one-to-one mapping between $\bar{a}$ and $\bar{p}$ is given as follows:

$$\bar{a}(t) = -\sqrt{\left(-\frac{2}{E^2A}\right)\left(\bar{p}(t) - \frac{1}{2A}\right)} + \frac{1}{EA}, \text{ when } \bar{a} \geq 0$$

$$\bar{a}(t) = -\sqrt{\left(+\frac{2}{E^2A}\right)\left(\bar{p}(t) + \frac{1}{2A}\right)} + \frac{1}{EA}, \text{ when } \bar{a} < 0$$

See Figs. 8(b) and 1(b) for the improved one-to-one mapping and the response. The response, being passive, is physically meaningful.

Such one-to-one mappings including those between a and p, a and S, and p and C and the subsequent "reset" to correct or improve the responses cannot be offered by mem-spring models using ξ as the state variable because ξ is neither a higher-order integral for ε nor a higher-order integral for σ. To assess the challenge of possibly changing the state variable from ξ to a when $n \neq 1$, we made the following manipulations:

$$\sigma = S\varepsilon_D, \quad \varepsilon_D = \frac{1}{S}\sigma \tag{19}$$

When $t = 0$, we have:

$$\varepsilon_D(0) = \frac{1}{S_0}\sigma(0) \tag{20}$$

Normalize the secant function as follows:

$$\varepsilon_D = \frac{1}{S_0}\frac{1}{\frac{S}{S_0}}\sigma \tag{21}$$

Contrasting with the 1-D CDM damage model:

$$\varepsilon_D = \frac{1}{E}\frac{1}{1-\xi}\sigma \tag{22}$$

and substituting Eq. (9) into (22), we have:

$$\varepsilon_D(t) = \frac{1}{E}\frac{1}{1 - AE^n\int_0^t (\dot{a}(\tau))^n\, d\tau}\sigma \tag{23}$$

Since we have $S_0 = E$, we have:

$$\frac{S}{S_0} = 1 - AE^n\int_0^t (\dot{a}(\tau))^n\, d\tau \text{ assuming } \xi(0) = 0 \tag{24}$$

We numerically verified that when $n \neq 1$, S is **not** even a function of both a and ε_D, making a simple time-invariant memcapacitive system model using a as a state variable impossible.

2.4 Possible 3-D Mem-Spring Model

A summary of CDM is given as follows. For 1-D, we have

$$\Psi(\varepsilon_D, \xi) = \frac{1}{2}E\varepsilon_D^2(1-\xi) \tag{25}$$

$$\sigma = \frac{\partial\Psi}{\partial\varepsilon_D} = E\varepsilon_D(1-\xi) \tag{26}$$

$$y = \frac{\partial\Psi}{\partial\xi} = -\frac{1}{2}E\varepsilon_D^2 = -\frac{1}{2E}\left(\frac{\sigma}{1-\xi}\right)^2 \tag{27}$$

$$\varepsilon_D = \frac{\sigma}{E(1-\xi)} \tag{28}$$

$$\dot{\xi} = A\left(\frac{\sigma}{1-\xi}\right)^n \tag{29}$$

where Ψ is the free energy (per unit volume of material), and y is the damage strain energy release rate (Lemaitre (1985)).

For 3-D and assuming isotropic damage, we have:

$$\Psi(\boldsymbol{\varepsilon}_D, \xi) = \frac{1}{2}\boldsymbol{\varepsilon}_D : \mathbb{E} : \boldsymbol{\varepsilon}_D(1-\xi) \tag{30}$$

$$\boldsymbol{\sigma} = \mathbb{E} : \boldsymbol{\varepsilon}_D(1-\xi) \tag{31}$$

$$y = \frac{\partial \Psi}{\partial \xi} = -\frac{1}{2}\boldsymbol{\varepsilon}_D : \mathbb{E} : \boldsymbol{\varepsilon}_D \tag{32}$$

$$\boldsymbol{\varepsilon}_D = \frac{\mathbb{E}^{-1} : \boldsymbol{\sigma}}{1-\xi} \tag{33}$$

$$\dot{\xi} \text{ to be discussed as follows,} \tag{34}$$

where $\boldsymbol{\varepsilon}_D$ and $\boldsymbol{\sigma}$ are now 3×3 symmetric second order tensors and $\mathbb{E}$ is the fourth order tensor of elasticity.

Damage equations under multiaxial stress conditions can be obtained by using an isotropic scalar-valued function $\chi(\boldsymbol{\sigma})$ of a symmetric second-order tensor, which can be approximated as a linear function of at most three invariants (forming irreducible basis functions). For example, following Chaboche (1987), we can have:

$$\chi(\boldsymbol{\sigma}) \;=\; \alpha I_0(\boldsymbol{\sigma}) + \beta I_1(\boldsymbol{\sigma}) + (1-\alpha-\beta) J_2(\boldsymbol{\sigma}), \tag{35}$$

where the maximum principal stress $I_0(\boldsymbol{\sigma}) = \sigma_1$, which opens the microcracks and causes them to grow. The hydrostatic stress $I_1(\boldsymbol{\sigma}) = \mathrm{Tr}(\boldsymbol{\sigma}) = \boldsymbol{\sigma} : 1$ greatly affects the growth of the cavities. The octahedral shear stress $J_2(\boldsymbol{\sigma})$ is related to the effects of deviatoric stress, and α and β are coefficients that depend on the material and temperature.

The missing Eq. (34) is recovered as follows:

$$\dot{\xi} = A\left(\frac{\chi(\boldsymbol{\sigma})}{1-\xi}\right)^n$$
$$\overset{\text{for example}}{=} A\left(\frac{\alpha I_0(\boldsymbol{\sigma}) + \beta I_1(\boldsymbol{\sigma}) + (1-\alpha-\beta) J_2(\boldsymbol{\sigma})}{1-\xi}\right)^n$$

The 3-D continuum damage mechanics (CDM) model is as follows:

$$\text{state equations:} \qquad \dot{\xi} = A\left(\frac{\chi(\boldsymbol{\sigma})}{1-\xi}\right)^n \tag{36}$$

$$\text{input-output equation:} \qquad \boldsymbol{\varepsilon}_D = \frac{\mathbb{E}^{-1} : \boldsymbol{\sigma}}{1-\xi} \tag{37}$$

where $A > 0$ and $n \geq 1$ are material properties. In this constitutive relation, the input is $\boldsymbol{\sigma}(t)$, while the output is $\boldsymbol{\varepsilon}_D(t)$ (damage strain). The input-output equation is no longer a scalar equation as in the definition for memristive system model in Chua and Kang (1976) and that for memcapacitive system model in Di Ventra et al (2009). The input-output equation is a tensorial equation, a necessary generalization from 1-D to 3-D.

We have thus reviewed both the 1-D and 3-D CDM formulas using $\Psi(\boldsymbol{\varepsilon}_D, \xi) = \frac{1}{2}\boldsymbol{\varepsilon}_D : \mathbb{E} : \boldsymbol{\varepsilon}_D(1-\xi)$ and $\boldsymbol{\sigma} = \mathbb{E} : \boldsymbol{\varepsilon}_D(1-\xi)$. We have shown that one specific 3-D mem-spring model can be obtained from the 3-D CDM theory. As far as we can tell, there are no previously published 3-D mem-spring models. Inspired by this particular case, a general effort-controlled memcapacitive system model in 3-D intended for material constitutive modeling may be expressed as follows:

$$\text{state equations:} \qquad \dot{\mathbf{y}}(t) = \mathbf{f}\left(\mathbf{y}(t), \boldsymbol{\sigma}(t), t\right) \tag{38}$$

$$\text{input-output equation:} \qquad \boldsymbol{\varepsilon}_D(t) = \mathbb{C}\left(\mathbf{y}(t), \boldsymbol{\sigma}(t), t\right) : \boldsymbol{\sigma}(t) \tag{39}$$

where $\mathbf{y}(t)$ is the state vector, $\boldsymbol{\sigma}(t)$ is the stress tensor, and $\varepsilon_D(t)$ is the strain tensor. In this constitutive relation, the input is $\boldsymbol{\sigma}(t)$, while the output is $\boldsymbol{\varepsilon}_D(t)$. $\mathbb{C}\left(\mathbf{y}(t), \boldsymbol{\sigma}(t), t\right) = \frac{\mathbb{E}^{-1}}{(1-\xi)}$, where $\mathbb{E}^{-1}$ stands for secant compliance matrix and can be seen as the inverse of the generalized spring stiffness, a function of the states and input.

For a given memcapacitive system, the absement, strictly speaking, is defined as the primitive of $\boldsymbol{\varepsilon}_D$, so it should be a symmetric second-order tensor $\mathbf{a}$ with $\dot{\mathbf{a}} = \boldsymbol{\varepsilon}_D$. If we want to adopt this point of view, by following more closely the 1-D case, we have the following for **an isotropic case**:

• 1-D: Using $\sigma = E\varepsilon_D(1-\xi)$ we have

$$\dot{\xi} = A\left(\frac{\sigma}{1-\xi}\right)^n = A(E\varepsilon_D)^n = A\left(E\dot{a}\right)^n$$

• 3-D: Using $\boldsymbol{\sigma} = \mathbb{E} : \boldsymbol{\varepsilon}_D(1-\xi)$ we have

$$\dot{\xi} = A\left(\frac{\chi(\boldsymbol{\sigma})}{1-\xi}\right)^n = A\left(\chi(\mathbb{E} : \boldsymbol{\varepsilon}_D)\right)^n = A\left(\chi(\mathbb{E} : \dot{\mathbf{a}})\right)^n,$$

where the absement is defined as $\dot{\mathbf{a}} = \boldsymbol{\varepsilon}_D$ and we assume that χ is a linear combination of stress invariants, as in (35).

2.5 Potential Connection with Hyperelasticity

Regarding the strain energy function, it was given in Pei et al (2015) for the simplest case of mem-springs and is rederived here for hyperelasticity (e.g., Houlsby and Puzrin (2007)):

$$\sigma = \frac{\partial \Psi}{\partial \varepsilon_D} \tag{40}$$

$$\sigma = S\left(\mathbf{y}, \varepsilon_D\right)\varepsilon_D \tag{41}$$

$$\frac{\partial \Psi}{\partial \varepsilon_D} = S\left(\mathbf{y}, \varepsilon_D\right)\varepsilon_D \tag{42}$$

for some free energy function $\Psi\left(\mathbf{y}, \varepsilon_D\right)$, where $\mathbf{y}$ is the state vector. The last equation legitimizes the internal variable-based strain energy function. Pei (2018) relaxes the continuity of S, thus making more options for Ψ possible. As in Pei

et al (2015), the simplest case would be as follows, still not allowing a closed-form solution:

$$\Psi = \int \sigma d\varepsilon_D = \int S(a)\varepsilon_D d\varepsilon_D \tag{43}$$

This is a very challenging topic calling for further studies. Other anecdotal facets are collected in Appendix A.1. With the challenge acknowledged, some preliminary thoughts are shared as follows:

For a flow-controlled setting in terms of $\sigma(t) = S(a(t))\varepsilon_D(t)$ and $p(t) = G(a(t))$, with $\dot{a}(t) = \varepsilon_D(t)$ and $\frac{dG}{da} = S$, we have:

$$\begin{aligned}
\Psi(t) &= \int \sigma(t) d\varepsilon_D(t) && (44)\\
&= \int S(a(t))\varepsilon_D(t) d\varepsilon_D(t) && (45)\\
&= \int S(a(t))\dot{\varepsilon}_D(t)\varepsilon_D(t) dt && (46)\\
&= \int \dot{\varepsilon}_D(t) S(a(t)) da(t) && (47)\\
&= \int \dot{\varepsilon}_D(t) dG(a(t)) && (48)\\
\Psi(t) &= \int \dot{\varepsilon}_D(t) dp(t) && (49)
\end{aligned}$$

Similarly, for an effort-controlled setting in terms of $\varepsilon_D(t) = C(p(t))\sigma(t)$ and $a(t) = F(p(t))$, with $\dot{p}(t) = \sigma(t)$ and $\frac{dF}{dp} = C$, we have:

$$\begin{aligned}
\Psi(t) &= \int \varepsilon_D(t) d\sigma(t) && (50)\\
&= \int C(p(t))\sigma(t) d\sigma(t) && (51)\\
&= \int C(p(t))\dot{\sigma}(t)\sigma(t) dt && (52)\\
&= \int \dot{\sigma}(t) C(p(t)) dp(t) && (53)\\
&= \int \dot{\sigma}(t) dF(p(t)) && (54)\\
\Psi(t) &= \int \dot{\sigma}(t) da(t) && (55)
\end{aligned}$$

Eqs. (49) and (55) are two forms of the energetics for a mechanical memcapacitor. For the special cases of $\varepsilon_D(t) = c_\varepsilon \mathcal{R}(t)$ and $\sigma(t) = c_\sigma \mathcal{R}(t)$ where $\mathcal{R}$ is the linear ramp function, we have the following expressions, respectively:

$$\Psi(t) = c_\varepsilon p(t), \;\; \Psi(t) = c_\sigma a(t) \tag{56}$$

which reveal a new insight into both absement and generalized momentum: **the energy can be either strain rate times generalized momentum, as in Eq.** (49)**, or stress rate times absement, as in Eq.** (55)**, in a strain- and stress-controlled setting, respectively.**

3 MEM-MODELS AND VISCOELASTICITY

3.1 Relationship between Ratcheting Strain and Generalized Momentum

Strain ratcheting refers to strain accumulation when the applied stress cycles have a non-zero mean stress, a.k.a., asymmetric stress (e.g., Moosbrugger and McDowell (1990); McDowell et al (1994)). Paul (2019) gives a recent review of ratcheting fatigue, where "ratcheting strain accumulation rate" plays an important role. See Fig. 9 for a numerical example developed in this study to produce a total of six different scenarios; the key statements made regarding the controlling factors for strain ratcheting in Paul (2019) are demonstrated as follows:

- The ratcheting strain accumulation rate is zero when the mean stress is zero. See Fig. 9(a). A counter-example is thermal expansion driven ratcheting, e.g. Bennett et al (2020).
- The ratcheting strain accumulation rate increases with the mean stress. Contrast Fig. 9(b) with Fig. 9(c).
- The ratcheting strain accumulation rate increases with the stress amplitude. Contrast Fig. 9(b) with Fig. 9(d). This may not be obvious visually, but the numerical values and Eq. (59) (later) support this claim.
- The ratcheting strain accumulation rate reduces with the increment in the stress rate. Contrast Fig. 9(b) with Fig. 9(e).
- The ratcheting strain accumulation rate is affected by the sign of the mean stress. Contrasting Fig. 9(b) with Fig. 9(f).

This numerical example was made by following Houslby et al (2017) in terms of (i) making the plastic strain and ratcheting strain additive; (ii) using a Masing model for the plastic deformation, and (iii) making the ratcheting strain a fraction of the plastic strain. In particular, the Masing model in Fig. 9(a) to (e) adopts the functional form of a virgin loading curve directly from Jayakumar (1987): $\varepsilon_M = -7.5 \ln\left(1 - \frac{\sigma}{2.5}\right)$, or equivalently, $\sigma = 2.5\left(1 - e^{-\frac{\varepsilon_M}{7.5}}\right)$, where the subscript M is for Masing model. The Masing model in Fig. 9(f) is simply anti-symmetric. The ratcheting strain is not introduced at the onset of the plastic strain. After the virgin loading curve is completed, the first unloading curve is finished, and when the reloading curve reaches the mean stress level, the ratcheting strain is started. This arrangement is purely meant to simplify the simulation by focusing on the new part of this study.

The new ideas in this study include (I) the use of generalized momentum, and (II) making ratcheting strain a static function of generalized momentum. What is presented in Fig. 9 is based on a linear relationship between ratcheting

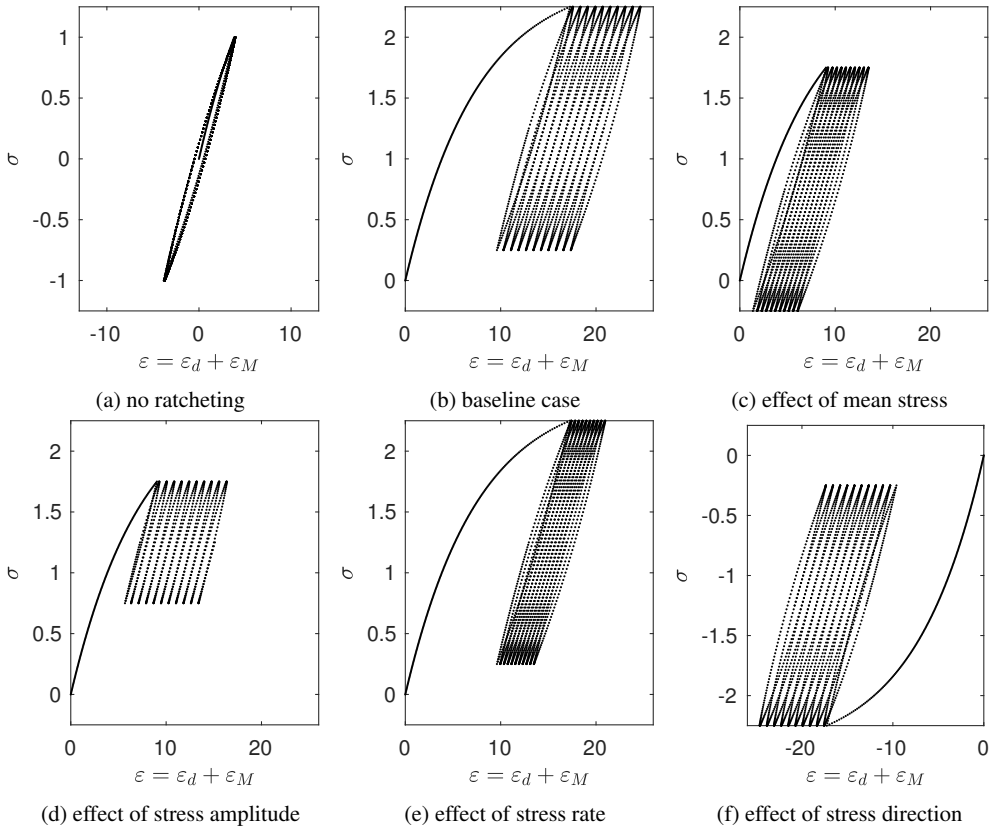

(a) no ratcheting (b) baseline case (c) effect of mean stress

(d) effect of stress amplitude (e) effect of stress rate (f) effect of stress direction

Fig. 9: Numerical example following Houslby et al (2017) for plastic and ratcheting strain additivity, with a Masing model for the plastic strain, and ratcheting as a fraction of plastic strain. We use the new ideas (in the main text) of (I) using generalized momentum, and (II) using a one-to-one mapping between the generalized momentum and ratcheting strain to make a mechanical memristor (here a linear function and so a linear dashpot only): the full stress-strain plots are given for all six scenarios (a) to (f)

strain and generalized momentum (in fact, a linear dashpot model); the choices of nonlinear functions will lead to the use of mechanical memristors, and will be given in Section 3.2.

Generalized momentum $p(t)$ is defined as the time integral of a stress time history $\sigma(t)$ following the naming in Pei et al (2018). For a periodic stress causing a strain ratcheting response, we have the following for the generalized momentum p as a function of time t:

$$p(t) = \int_0^t \left(\sigma_0 \sin(\omega\tau) + \bar{\sigma}\right) d\tau \tag{57}$$

$$= \frac{\sigma_0}{\omega}\left(1 - \cos\left(\omega t\right)\right) + \bar{\sigma}t, \tag{58}$$

where σ_0 is the stress amplitude with $\sigma_0 \geq 0$, $\bar{\sigma}$ is the mean stress, and ω is the stress angular frequency. See Fig. 10 for the time histories of $p(t)$ corresponding to all six scenarios in Fig. 9 where T is the period of the stress; the numerical values used for $\bar{\sigma}$, σ_0, and ω for each scenario are given in Table 3.

There is a periodic component and a linear component in $p(t)$, making the understanding of $p(t)$ a little obscure. If we track the maxima in a $\sigma(t)$ time history, then we collect the time instants when $\omega t = \frac{(4n+1)\pi}{2}$ with $n \in \mathbb{N}$. Defining these special time instants as $t_n = \frac{(4n+1)\pi}{2\omega}$, we have:

$$p\left(t_n\right) = \frac{\sigma_0}{\omega} + \bar{\sigma}t_n \tag{59}$$

which is for a specific value of n. Holding n constant, it can be seen that

- When $\bar{\sigma} = 0$, $p\left(t_n\right)$ is a constant with respect to t_n.
- When $\bar{\sigma} > 0$, $p\left(t_n\right)$ increases with t_n.
- When σ_0 increases, $p\left(t_n\right)$ increases uniformly.
- When ω increases, $p\left(t_n\right)$ decreases uniformly.
- When $\bar{\sigma} < 0$, $p\left(t_n\right)$ decreases with t_n and will eventually change its sign.

Table 3: Numerical values of the parameters in Figs. 9 and 10

Scenario ID	$\bar{\sigma}$	σ_0	ω
(a)	0	1	1
(b)	1.25	1	1
(c)	0.75	1	1
(d)	1.25	0.5	1
(e)	1.25	1	2
(f)	-1.25	1	1

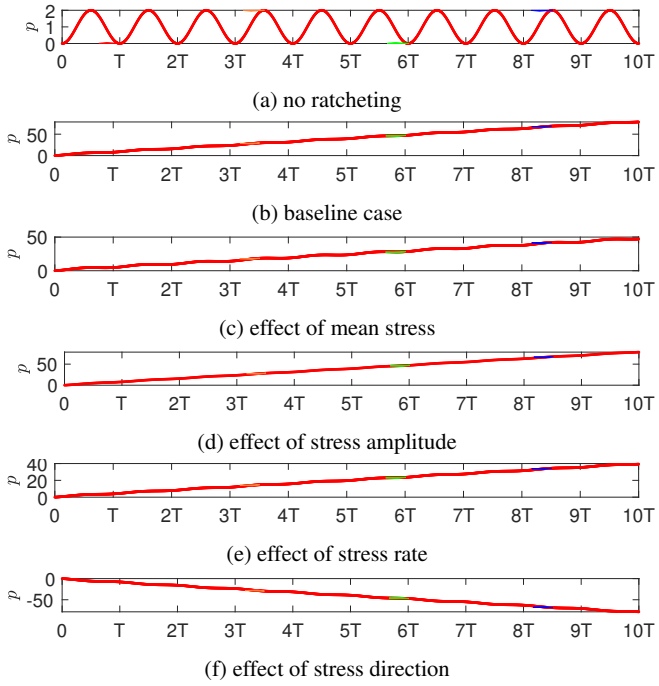

Fig. 10: Same numerical example following Houslby et al (2017) as in Fig. 9: the time histories of generalized momentum as given for all six scenarios (a) to (f)

Now, it can be seen that $p(t_n)$ correlates well with "ratcheting strain accumulation rate". Moreover, $p(t_n)$ is a quantitative measure. We directly apply the generalized momentum concept in the mem-modeling. We follow the "higher-order element" (HOE) (Chua (2003); Biolek et al (2016)), which is another general theory that overlaps with the mem-models. Like absement, a negative higher-order kinematic quantity than the velocity or strain rate itself, generalized momentum is simply a negative higher-order kinetic quantity than the characteristic force or stress itself.

3.2 Potential Role of Memristor in Modeling Strain Ratcheting and More

The strain ratcheting literature indicates the necessity for constant, decreasing, and increasing ratcheting rate, e.g., see Fig. 3 in Paul (2019). Eq. (59) indicates a linear relationship of the time instants t_n (corresponding to the maxima in $\sigma(t)$) and $p(t)$. This means that a constant ratcheting rate can be realized by using a linear mapping between generalized momentum $p(t)$ and ratcheting strain $\varepsilon(t)$ in the following two equivalent definitions through time differentiation:

$$\varepsilon_d(t) = wp(t), \quad \dot{\varepsilon}_d(t) = w\sigma(t), \tag{60}$$

where ε_d is ratcheting strain. w is the reciprocal of the viscosity of the linear dashpot; the results given previously in Fig. 9 use $w = 0.1$.

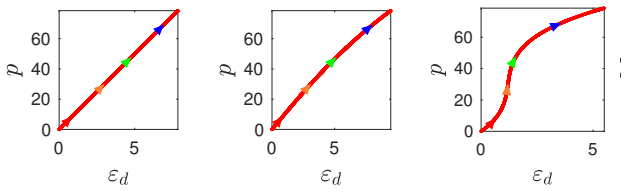

(a) linear dashpot for Fig. 9 (b) softening memristor for Fig. 2(a) (c) hardening-softening memristor for Fig. 2(b)

Fig. 11: One-to-one mappings between the generalized momentum and ratcheting strain to make mechanical memristors

A time-varying ratcheting rate can be realized through a nonlinear mapping between generalized momentum $p(t)$ and ratcheting strain $\varepsilon_d(t)$ in the following two equivalent definitions through time differentiation:

$$\varepsilon_d(t) = F\left(p(t)\right), \quad \dot{\varepsilon}_d(t) = \frac{dF(p(t))}{dp}\sigma(t), \tag{61}$$

where $\frac{dF(p)}{dp} = W(p)$ leading to $\dot{\varepsilon}_d(t) = W\left(p(t)\right)\sigma(t)$, a differential form for a mechanical memristor. Fig. 2(a) and (b) give two examples of memristor-based ratcheting responses with $W(p) = 0.1 + \frac{p^2}{100000}$ and $W = 0.01 + \frac{(p-30)^2}{10000}$, respectively. Their nonlinear mappings between $p(t)$ and $\varepsilon_d(t)$, as well as $w = 0.1$ for the linear mapping discussed above, are given in Fig. 11.

The plastic and ratcheting strain and their sum for these three models for Scenario (b) in Table 3 is given column-wise in Fig. 12. The time in Fig. 12 is a delayed time compared with Fig. 9 given the choice of the start of the ratcheting strain.

Generalized momentum $p(t)$ is exploited here as a surrogate for time parameterization, based on the mem-modeling given in Pei (2018). Time, or equivalently number of cycles, can be replaced with generalized momentum, after which characteristic curves of ratcheting strain versus number of cycles could be used to determine the one-to-one mapping between generalized momentum $p(t)$ and ratcheting strain $\varepsilon(t)$. In fact, this mem-model mode of thinking - namely exploiting a one-to-one p versus ε mapping - was instumental in constructing all examples on the topic presented here.

Having explored a mechanical memristor to model ratcheting strain, let us examine whether a mechanical memristor has more modeling potential for a viscosity-hardening law. Following Section 6.2.4 in Lemaitre and Chaboche (1990), the viscosity-hardening law can be written as:

$$\sigma = K\varepsilon_p^{1/M}\dot{\varepsilon}_p^{1/N}, \tag{62}$$

where ε_p is the plastic strain, and N, M and K are three parameters that are functions of temperature and depend on the material. It can be seen that the hardening-law is based on a

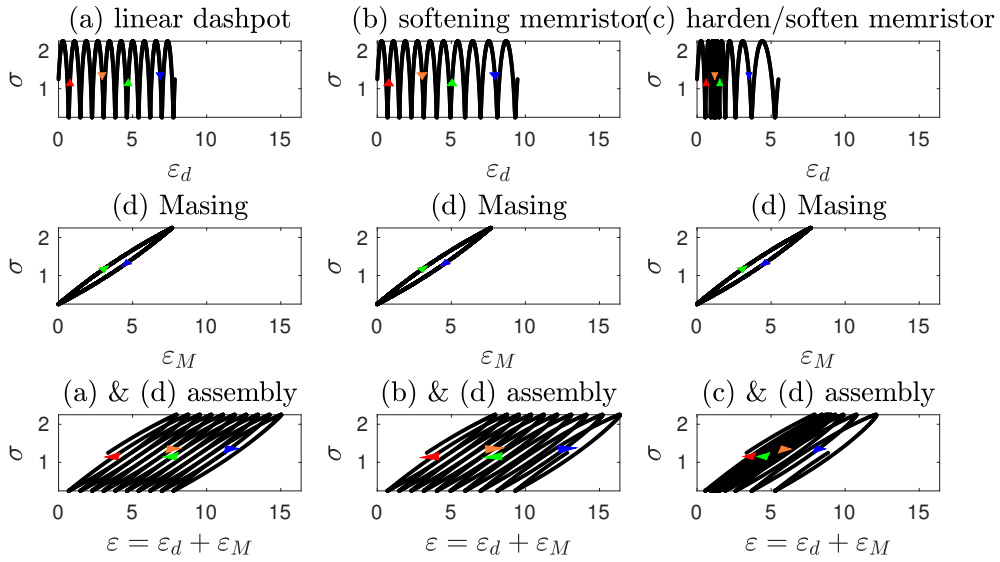

Fig. 12: Same numerical example following Houslby et al (2017) as in Figs. 9 and 10. The one-to-one mapping between the generalized momentum and ratcheting strain to make a mechanical memristor follow the three choices of (a) to (c) going from the left to right columns in Fig. 11. The stress-strain plots are given for ratcheting strain only under Scenario (b) in Table 3. Note that the time here is a delayed time compared with Fig. 9 given the the choice of the start of the ratcheting strain there

flow-controlled time-invariant memristive system model

$$\sigma \;=\; D\left(\varepsilon, \dot{\varepsilon}_p\right) \dot{\varepsilon}_p \tag{63}$$

Pei (2018) explores both the creep and relaxation responses of a mechanical memcapacitor. Here we discuss creep, relaxation, and ramped strain responses of a mechanical memristor defined previously in Eq. (61) with the subscript d replaced with p. The desired responses are depicted in Figs. 6.11, 6.25 and 6.26 in Lemaitre and Chaboche (1990), respectively. Some simple derivations are presented, along with a numerical example using $W(p) = \frac{6}{1+e^p} + 1$.

– First, we subject this memristor model to a creep test where $\sigma(t) = c\sigma_0\mathcal{H}(t)$, where $c \in \mathbb{R}$ and $\mathcal{H}(t)$ is the Heaviside function. We then have $p(t) = c\sigma_0\mathcal{R}(t)$ where $\mathcal{R}$ is the linear ramp function. We have:

$$\dot{\varepsilon}_p(t) = W(p)\sigma(t) \tag{64}$$
$$= W(c\sigma_0\mathcal{R}(t))c\sigma_0\mathcal{H}(t) \tag{65}$$
$$\varepsilon_p(t) = F\left(c\sigma_0\mathcal{R}(t)\right) \tag{66}$$

This reveals what creep responses mean for a memristor. Comparison with Fig. 6.11 in Lemaitre and Chaboche (1990) is given in Fig. 13(a).

– Relaxation response, however, cannot be captured well by using one memristor model alone given $\sigma(t) = D(\varepsilon_p(t))\dot{\varepsilon}_p(t)$ with $\varepsilon_p(t) = c\varepsilon_0\mathcal{H}(t)$ and $\dot{\varepsilon}_p(t) = c\varepsilon_0\delta(t)$, where $\delta(t)$ stands for Dirac delta function, making the response non-physical, the same difficulty as with a linear dashpot. Note that D is the inverse function of W.

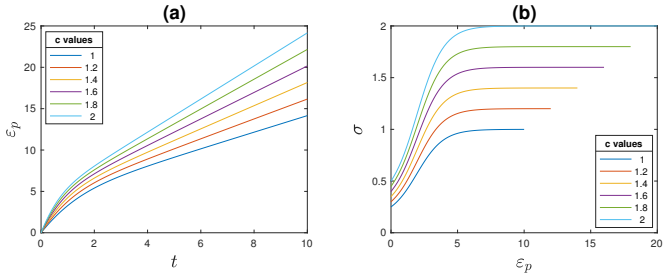

Fig. 13: Responses generated by a mechanical memristor defined by $W(p) = \frac{6}{1+e^p} + 1$: (a) mimicking Fig. 6.11 in Lemaitre and Chaboche (1990), and (b) mimicking Fig. 6.26 in Lemaitre and Chaboche (1990)

– Finally, we study how this memristor would respond to ramped strain inputs with various strain rates in comparison with Fig. 6.26 in Lemaitre and Chaboche (1990):

$$\sigma(t) \;=\; D(\varepsilon_p(t))\dot{\varepsilon}_p(t) \tag{67}$$

When $\varepsilon_p(t) = c\mathcal{R}(t)$, we have $\dot{\varepsilon}_p(t) = c\mathcal{H}(t)$, and

$$\sigma(t) = D(c\mathcal{R}(t))c\mathcal{H}(t) \tag{68}$$
$$p(t) = G(c\mathcal{R}(t)) \tag{69}$$

See Fig. 13(b), which exhibits some discrepancies from Fig. 6.26 in Lemaitre and Chaboche (1990). Various facets behind Fig. 13(b) are plotted in Fig. 14. Since D (hence W) is nonnegative, this is a passive mechanical memristor, in accord with the passivity property in Chua and Kang (1976). Thus, all these are one-to-one mappings. Different strain rates do "activate" different ranges in each one-to-one mapping. Nonetheless, it can

be seen that W is the slope of ε_p-p and D is the slope of p-ε_p. The inverse relationship between W and D can be seen as well.

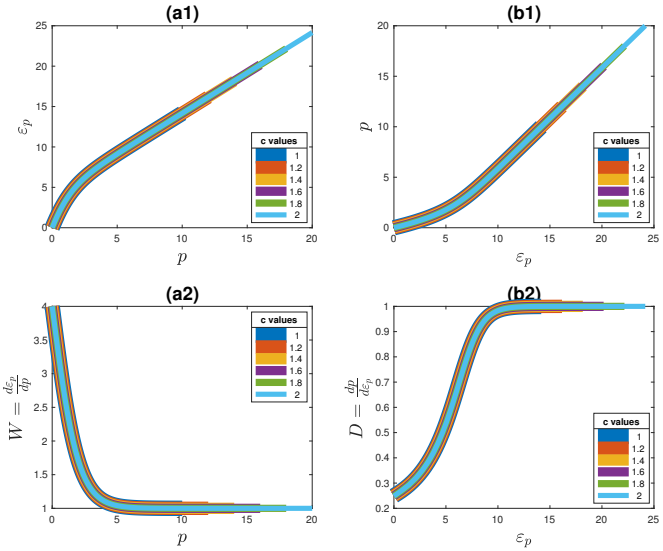

Fig. 14: One-to-one mappings of a mechanical memristor defined by $W(p(t)) = \frac{6}{1+e^{p(t)}} + 1$ subject to $\varepsilon_p(t) = c\mathcal{R}(t)$ with six different strain rates c shown in the legend

The modeling power of an individual memristor for creep, relaxation, and ramped strain responses thus seems limited, which prompts the next topic.

3.3 Memristor and Memcapacitor Connected in Series

Assembling elementary models to make more complex models has been a powerful approach in modeling representation. Following bond graph theory, flow-controlled, effort-controlled and mixed assemblies, corresponding to connectivities in parallel, series, and both, respectively, have been used in mem-modeling (Jeltsema and Scherpen (2009)). In this study, connecting in series a mechanical memristor for ratcheting strain and a Masing model for plastic strain makes it efficient to capture strain ratcheting response under an asymmetric periodic stress, i.e., $\varepsilon = \varepsilon_d + \varepsilon_M$. Another example for model assembly is the relation $\varepsilon = \varepsilon_e + \varepsilon_p$ in the literature (e.g., Lemaitre and Chaboche (1990)) for the total strain as a summation of linear elastic strain and plastic strain. Pei et al (2020a) introduces a means of exercising various mem-springs connected in series with various mem-dashpots; see Figs. 8 to 11 there for numerical examples. An identification scheme is discussed there as well.

Having previously compared a mem-model assembly with a Maxwell model (with two model parameters) in Pei et al (2020a), **we are curious to learn how the responses of a mem-model assembly (one mem-spring and one mem-dashpot connected in series) and a popular linear model assembly (a Wiechert model with two arms) would differ from each other. To make a tangible comparison, we start with the same creep response for the two types of models and proceed to compare their sinusoidal response and one specific strain ratcheting response.**

For a Wiechert model subject to stress inputs, we have the Voigt type as illustrated in Fig. 15 and its creep compliance function as follows (when $\sigma(t) = \sigma_0\mathcal{H}(t)$):

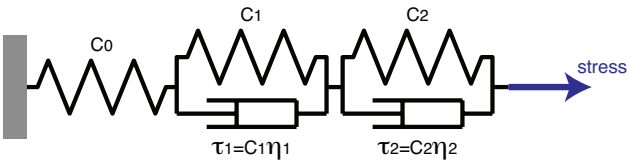

Fig. 15: Voigt type Wiechert model following Roylance (2001) where $C = 1/E$, and $\tau = \frac{\eta}{E}$

$$C_{\text{creep}}(t) = \frac{\varepsilon(t)}{\sigma_0} = C_0 + \sum_j C_i \left(1 - e^{-\frac{t}{\tau_j}}\right), \tag{70}$$

where $\tau_j = \frac{\eta_j}{E_j}$, with j the number of the Kelvin arms. We will restrict to the case of $j = 2$ herein for demonstration purposes. Three sets of parameter values are chosen as listed in Table 4; their corresponding creep response time histories in log scale are plotted in Fig. 16, where Cases 2 and 3 display two inflection points corresponding to $j = 2$.

Table 4: Numerical values of the parameters in Eq. (70)

Case ID	C_0	C_1	τ_1	C_2	τ_2	σ_0
1	1	1	1	1	1	1
2	1	1	0.1	1	5	1
3	1	1	0.5	2	20	1

We use a mem-spring to match the creep response of the standard solid part of the Wiechert model. We use a memristor to match the creep response of the remaining Kelvin arm. The total and individual targeted responses are given as follows:

$$\varepsilon(t) = \varepsilon_s(t) + \varepsilon_d(t) \tag{71}$$

$$\varepsilon_s(t) = \left[C_0 + C_1\left(1 - e^{-\frac{t}{\tau 1}}\right)\right]\sigma_0\mathcal{H}(t) \tag{72}$$

$$\varepsilon_d(t) = C_2\left(1 - e^{-\frac{t}{\tau_2}}\right)\sigma_0\mathcal{H}(t), \tag{73}$$

where the subscripts s and d represent mem-spring and mem-dashpot, respectively.

For the mem-spring, we apply $p(t) = \sigma_0\mathcal{R}(t)$ to the manipulation to obtain the following:

$$\varepsilon_s(t) = \left[C_0 + C_1\left(1 - e^{-\frac{p(t)}{\sigma_0\tau 1}}\right)\right]\sigma(t) \tag{74}$$

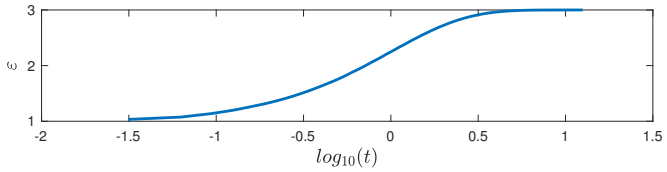

(a) Case 1 in Table 4

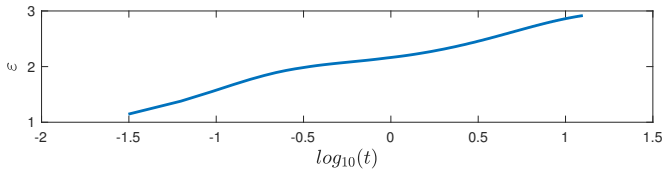

(b) Case 2 in Table 4

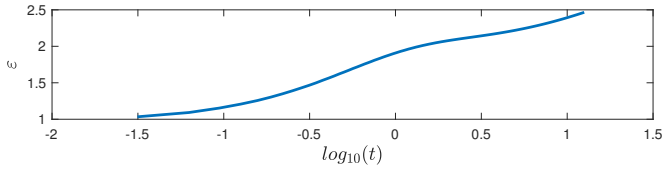

(c) Case 3 in Table 4

Fig. 16: Creep responses plotted in log scale for time

This is the model for the mem-spring that we are seeking in terms of $\varepsilon(t) = C\left(p(t)\right)\sigma(t)$, where $C(p) = \left[C_0 + C_1\left(1 - e^{-\frac{p}{\sigma_0 \tau_1}}\right)\right]$. This is an effort-controlled mechanical memcapacitor model, which would generate energy if loaded in the opposite direction in a sinusoidal test (Pei et al (2015); Pei (2018)). Therefore, as was previously done in Section 2.3, the integrations of ε_s and σ for a and p will be reset into $\bar{a}$ and $\bar{p}$, respectively, whenever the loading changes its direction. The one-to-one mappings between $\bar{a}$ and $\bar{p}$ in two directions are made anti-symmetrical. Using Case 2 in Table 4 as an example, Fig. 17(a) presents various facets of the mem-spring model with σ-ε_s as a loop, $\bar{p}$-$\bar{a}$ being one-to-one and anti-symmetrical, and both S-$\bar{a}$ and C-$\bar{p}$ being one-to-one and symmetrical.

For the mem-dashpot, we have the following step:

$$\begin{aligned}\varepsilon_d(t) &= C_2\left(1 - e^{-\frac{t}{\tau_2}}\right)\sigma_0\mathcal{H}(t)\\ &= C_2\left(1 - e^{-\frac{\sigma_0\mathcal{R}(t)}{\sigma_0\tau_2}}\right)\sigma_0\mathcal{H}(t)\\ &= C_2\left(1 - e^{-\frac{p(t)}{\sigma_0\tau_2}}\right)\sigma_0, \quad \text{when } t \geq 0\end{aligned}$$

so

$$\dot{\varepsilon}_d(t) = \frac{C_2}{\tau_2}e^{-\frac{p(t)}{\sigma_0\tau_2}}\sigma(t), \quad \text{when } t \geq 0 \tag{75}$$

This is the model for a mechanical memristor that we are seeking in terms of $\dot{\varepsilon}(t) = W\left(p(t)\right)\sigma(t)$, where $W(p) = \frac{C_2}{\tau_2}e^{-\frac{p}{\sigma_0\tau_2}}$. Using Case 2 in Table 4 as an example, Fig. 17(b) presents various facets of the mechanical memristor model with σ-$\dot{\varepsilon}_d$ as a loop, and p-ε_d, D-ε_d and W-p all being one-to-one.

In both Figs. 18 and 19, there are three columns progressing through a Maxwell model, a two-arm Wiechert model, and a mem-model assembly consisting of a mem-spring and a mem-dashpot. These three different kinds of models are contrasted in terms of both sinusoidal and strain ratcheting responses. The parameters of these model are tuned as specified in the captions to enable a more reasonable comparison. Such model calibrations are exercised for both Kelvin and Maxwell models with each using a mechanical memcapacitor subject to a sawtooth input; this is presented in Appendix A.2 where fundamental differences can be seen between mem-spring models and classical linear models (with two parameters each).

It can be seen that the Wiechert models lead to richer linear responses than their Maxwell model counterparts. The nonlinear responses of the mem-model assemblies are the richest, hopefully mimicking some meaningful responses of real-world applications. Again, fundamental differences can be seen between mem-models and classical linear models.

4 CONSTRUCTING MEM-SPRINGS WITH CLASSICAL PREISACH MODELS

4.1 Subset of Classical Preisach Models

We assume that there exists a classical Preisach model that satisfies the origin-crossing property of the mem-models, i.e., the input and output become zero simultaneously (e.g., Song et al (2001)). It will be shown that this subset of the classical Preisach model can be transformed into an equivalent time-invariant memcapacitive system model.

Making this happen has two important practical implications. First, the identification and inversion of the classical Preisach model is computationally demanding, while the identification and inversion of the time-invariant mem-models is much less so. Second, the classical Preisach model is considered a hysteresis operator confined within its own rules and notations, while the mem-spring models fall under the category of differential models, preferably using the notation of hybrid dynamical system theory, and with a demonstrated possibility of providing physical interpretations and quantities that are enabled by a higher-order framework affecting the choice of state variables.

The classical Preisach models are probably the most celebrated hysteresis models. Mayergoyz (2003) contains a comprehensive description of these models, which were originally developed for magnetic hysteresis (Preisach (1935); Krasnosel'skii and Pokrovskii (1989)) but are more general. These models are made up of piecewise monotonically increasing or decreasing input-output branches (e.g., Mayergoyz (2003)). This is consistent with "monotone operators" and discussions on "vibro-correctness" in Krasnosel'skii and Pokrovskii (1989). The input-output relation

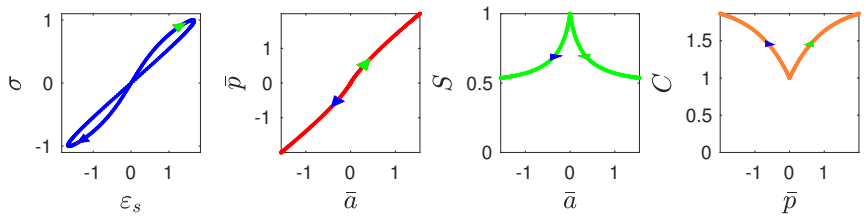

(a) mem-spring

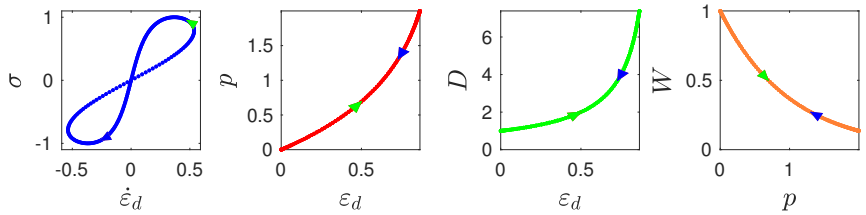

(b) mem-dashpot (mechanical memristor)

Fig. 17: Behaviors of the mem-spring and mem-dashpot in Case 2 of Table 4, whose serial connection is calibrated against (in terms of creep response according to Eqs. (71), (74) and (75)) and to be compared with a two-arm Wiechert model in terms of sinusoidal and strain ratcheting test

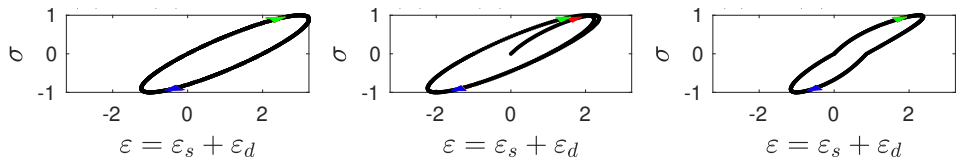

(a) Case 1 in Table 4

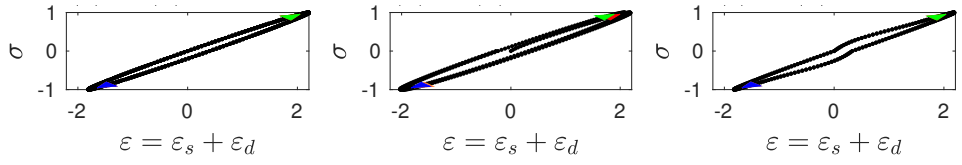

(b) Case 2 in Table 4

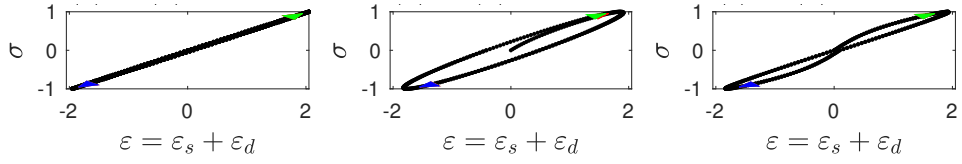

(c) Case 3 in Table 4

Fig. 18: Sinusoidal responses of three different assemblies. Column-wise, they are a spring with $C_0 + C_1$ connected in series with a linear dashpot with τ_2; the Wiechert model with two arms defined in Eqs. (71), (72) and (73), and the mem-model assembly defined in Eqs. (71), (74) and (75)

of the classical Preisach model is given as follows:

$$y(t) = \iint_T \nu(\alpha, \beta)\, \mathcal{R}_{\alpha,\beta} u(t) d\alpha d\beta, \tag{76}$$

where $u(t)$ and $y(t)$ are the input, and output, respectively. $\mathcal{R}_{\alpha,\beta}$ represents a relay hysteron operator with switching down and up thresholds as α and β, respectively; $\nu(\alpha, \beta)$ is the Preisach (density, weighting, distribution) function; T denotes the Preisach triangle with $\beta \geq \alpha$. See Fig. 20.

In the classical Preisach model, to determine the weighing function $\nu(\alpha, \beta)$, one of the two options is to start with a limiting ascending branch as in Fig. 20(a). Then, a set of first-order transition curves is attached to this limiting ascending branch as in Fig. 20(b). In this figure, the shaded area S^+ inside the Preisach triangle has the relay hysteron operator switched "on" corresponding to $\mathcal{R}_{\alpha,\beta} u(t) = 1$ for that particular time instant. The unshaded area S^- inside the Preisach triangle has the relay hysteron operator switched "off" corresponding to $\mathcal{R}_{\alpha,\beta} u(t) = -1$ for that particular time instant. This leads to:

$$y(t) = \iint_{S^+} \nu(\alpha, \beta)\, d\alpha d\beta - \iint_{S^-} \nu(\alpha, \beta)\, d\alpha d\beta \tag{77}$$

The following formulation is general from Mayergoyz (2003), but we focus on the subset of the classical Preisach model illustrated in Fig. 21(a). Define $F(\alpha', \beta')$ as follows:

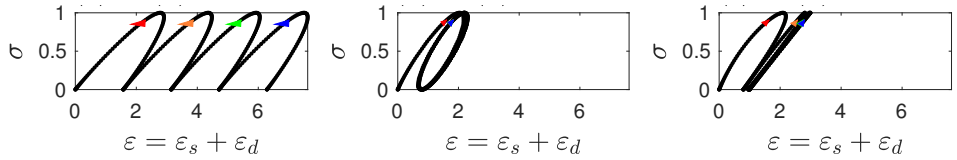

(a) Case 1 in Table 4

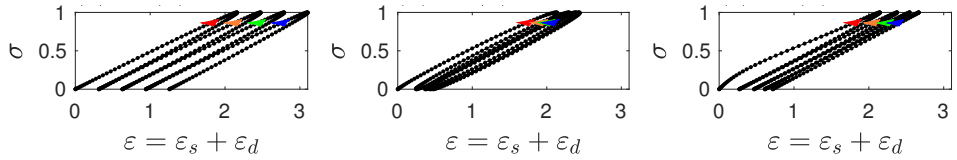

(b) Case 2 in Table 4

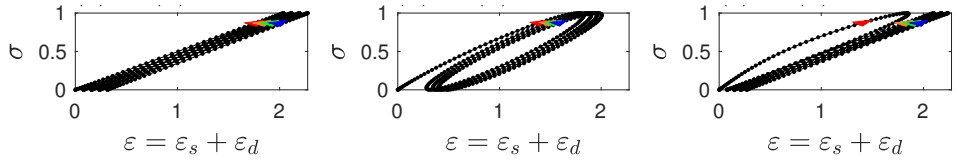

(c) Case 3 in Table 4

Fig. 19: Sinusoidal responses of three different assemblies. Column-wise, they area spring with $C_0 + C_1$ connected in series with a linear dashpot with τ_2; the Wiechert model with two arms defined in Eqs. (71), (72) and (73), and the mem-model assembly defined in Eqs. (71), (74) and (75)

$$F(\alpha', \beta') \;=\; \frac{f_{\alpha'} - f_{\alpha'\beta'}}{2}, \tag{78}$$

where the input α' is on the limiting ascending branch, and its output is $f_{\alpha'}$. The input β' is on a first-order descending branch that starts to descend from α'; the output corresponding to this β' is denoted as $f_{\alpha'\beta'}$. It can be shown that:

$$F(\alpha', \beta') \;=\; \int_{\beta'}^{\alpha'} \left(\int_{\beta}^{\alpha'} \nu(\alpha, \beta) d\alpha \right) d\beta \tag{79}$$

from which, it can be derived that:

$$\nu(\alpha', \beta') \;=\; -\frac{\partial^2 F(\alpha', \beta')}{\partial \alpha' \partial \beta'} \tag{80}$$

4.2 Constructing Mem-Springs using Preisach Model

We choose an effort-controlled mem-spring model in Fig. 21(b) that can be equivalently represented by a classical Preisach model in Fig. 21(a). We desire the following state and input/output equations for this time-invariant effort-controlled memcapacitive system model:

$$\dot{\mathbf{y}}(t) = \mathbf{f}\left(\mathbf{y}(t), r(t)\right) \tag{81}$$

$$x(t) = W\left(\mathbf{y}(t), r(t)\right) r(t) \tag{82}$$

from which we have

$$W\left(\mathbf{y}, r\right) \;=\; \frac{x}{r} \tag{83}$$

First, on the loading branch, because $(\alpha',\ f_{\alpha'})$ is on the limiting ascending branch of the Preisach model, we have from Eq. (77):

$$f_{\alpha'} = \int_{-\infty}^{\alpha'} \left(\int_{-\infty}^{\alpha} \nu(\alpha, \beta) d\beta \right) d\alpha - \int_{\alpha'}^{+\infty} \left(\int_{-\infty}^{\alpha} \nu(\alpha, \beta) d\beta \right) d\alpha \tag{84}$$

This is a zero-crossing for x as a function of r with $r = \alpha'$. There is no need for a state variable, and $W = \tilde{W}(r)r$ would suffice. So, we focus on the unloading branch, i.e., a first-order reversal curve. Using Fig. 21(b), we have the following expression for the secant stiffness of a generic point on the descending branch:

$$W(\alpha', \beta') \;=\; \frac{f_{\alpha'\beta'}}{\beta'} \tag{85}$$

From Eq. (78), we have:

$$f_{\alpha'\beta'} = f_{\alpha'} - 2F(\alpha', \beta') \tag{86}$$

Substituting both Eqs. (84) and (79) into (86), it can be seen that the numerator of the secant stiffness function $W(\alpha', \beta')$ contains double integrals of the Preisach density function ν. Next, we convert α' and β' into the input and state variables. For the first-order reversal curve, we have $r = \beta'$. We have two options of introducing the state variable.

Under the first option, we follow Gurtin and Francis (1981) and Pei (2018) by introducing a maximum force r_m used to track the limiting ascending branch for this effort-controlled setting. In a a flow-controlled setting in Gurtin and Francis (1981) and Pei (2018), there is a maximum displacement. Then, we have $r_m = \alpha'$. With this, we have:

$$W(\alpha', \beta') = W(r_m, r),$$

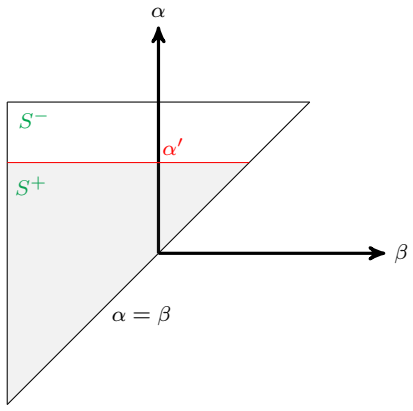

(a) limiting ascending branch

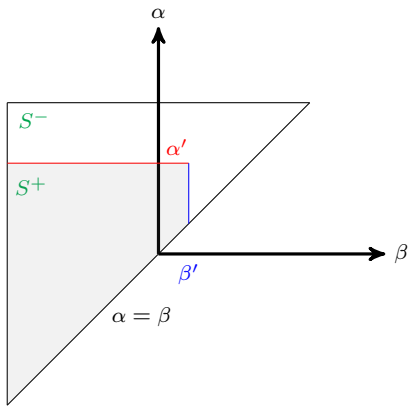

(b) first-order reversal curve

Fig. 20: Preisach plane

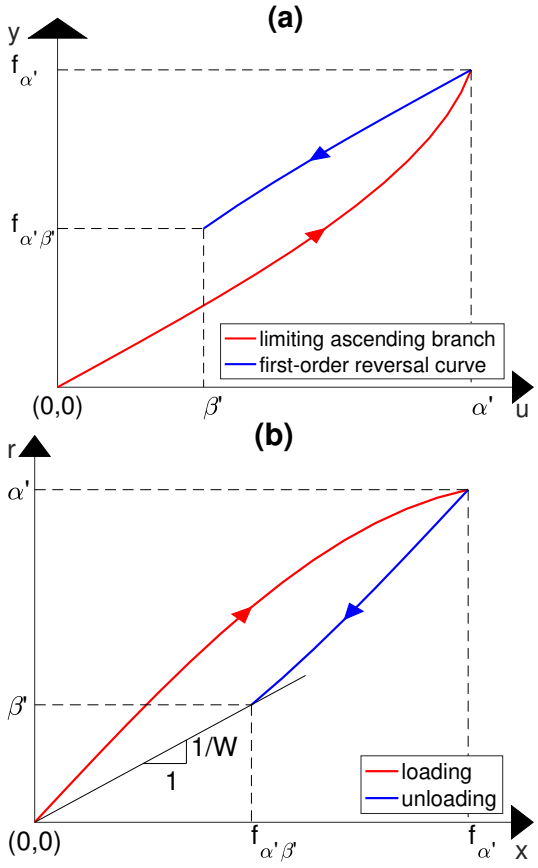

Fig. 21: Input-output plot of a mem-spring in terms of (a) a classical Preisach model, and (b) a mem-spring model

where

$$W(r_m, r) = \frac{\text{1st integral + 2nd integral + 3rd integral}}{r}$$

$$\text{1st integral} = \int_{-\infty}^{r_m} \left(\int_{-\infty}^{\alpha} \nu(\alpha, \beta) d\beta \right) d\alpha$$

$$\text{2nd integral} = -\int_{r_m}^{+\infty} \left(\int_{-\infty}^{\alpha} \nu(\alpha, \beta) d\beta \right) d\alpha$$

$$\text{3rd integral} = -2 \int_{r}^{r_m} \left(\int_{\beta}^{r_m} \nu(\alpha, \beta) d\alpha \right) d\beta$$

This applies to the first-order reversal curve. For the limiting ascending branch, this also applies because $r_m = r$ and the third integral vanishes.

By following Pei (2018), we have the following discrete-time state equation for both branches:

$$r_m(k+1) = \max(r_m(k), r(k+1)), \text{ with } r_m(1) = r(1)$$

which can be rewritten into a continuous-time format. With this, we have constructed a time-invariant memcapacitive system model as follows:

$$\dot{r}_m = f(r_m, r) \tag{87}$$

$$x = W(r_m, r) r \tag{88}$$

This formulation, in fact, is more general than that in Pei (2018) based on Gurtin and Francis (1981). A strong limitation is that this formulation only applies to both the limiting ascending branch and first-order reversal curve. More state variables are needed to track the first-, second-, etc. order reversal curve(s) when higher-order reversal curves are anticipated in the output.

The second option is taken in an approximate sense. Assuming loading and unloading follows a constant loading rate, we have:

$$p = \alpha' \frac{T}{2} - \frac{\beta' \frac{\beta'}{\alpha'} \frac{T}{2}}{2}, \tag{89}$$

where p is the generalized momentum in Pei et al (2018), and T is the duration of one loading cycle. It can be seen that α' can be solved in terms of β' and p. This leads to the following:

$$W(\alpha, \beta) = \bar{W}(p, r) \tag{90}$$

In summary, when we can assume loading and unloading with a constant loading rate, we have:

$$\dot{p} = r \tag{91}$$

$$x = \bar{W}(p, r) r \tag{92}$$

which has the same strong limitation as the first option.

We note that the Masing model used to generate the plastic strain in Section 3.1 could be reformulated in terms of a mem-spring by applying a slightly extended version of the methodologies presented above. The complete model to capture strain ratcheting could then involve a mem-model assembly with one mem-spring and one mem-dashpot connected in series.

5 DUHEM MODELS

Here we examine a possible connection between the generalized Duhem model and the mem-models. From Padthe et al (2008), we have the following definition (*begin quote*):

$$\dot{x}(t) = f\left(x(t), u(t)\right) g\left(\dot{u}(t)\right), \;\; x(0) = x_0, \;\; t \geq 0 \tag{93}$$

$$y(t) = h\left(x(t), u(t)\right), \tag{94}$$

where $x : [0, \infty) \rightarrow \mathbb{R}^n$ is absolutely continuous, $u : [0, \infty) \rightarrow \mathbb{R}$ is continuous and piecewise $\mathcal{C}^1$, $f : \mathbb{R}^n \times \mathbb{R} \rightarrow \mathbb{R}^{n \times r}$ is continuous, $g : \mathbb{R} \rightarrow \mathbb{R}^r$ is continuous and satisfies $g(0) = 0$ and $y : [0, \infty) \rightarrow \mathbb{R}$, and $h : \mathbb{R}^n \times \mathbb{R} \rightarrow \mathbb{R}$ are continuous. The value of $\dot{x}$ at a point t at which $\dot{u}$ does not exist can be assigned arbitrarily. We assume that the solution to Eq. (93) exists and is unique on all finite intervals. Under these assumptions, x and y are continuous and piecewise $\mathcal{C}^1$. ... Assume that g is positively homogeneous, that is

$$g(\alpha v) = \alpha g(v), \; \forall \alpha > 0 \text{ and } v \in \mathbb{R} \tag{95}$$

then, the generalized Duhem model in Eqs. (93) and (94) is rate-independent (*end quote*).

It can be seen that under this condition and assuming x is a state variable, Eq. (93) becomes a differential form of the mem-model in Pei et al (2018). Eq. (93) thus has zero-crossing and rate-independence. This is one connection between the generalized Duhem and mem-models. A difference is that zero-crossing is a property of the vector state equation rather than the scalar input-output equation.

6 CONCLUSIONS

Mem-models are a family of new models of dampers, springs, inerters (and very likely, more) originally based on nonlinear state-space representations. However, how to choose state variables and define functional forms for mem-models is unspecified and remains a major technical challenge. The connections made herein suggest specific and potentially fruitful paths to search for state variables and functional forms for mem-springs. One choice makes mem-springs physically meaningful in modeling the basic kind of damage that is defined and involved in continuum damage mechanics (CDM) context. We also generalize mem-springs from 1-D to 3-D for isotropic materials for future work to validate. Tapping functional forms from viscoelasticity is constructive and fruitful, however bear in mind that mem-models are fundamentally nonlinear and thus are fundamentally different from classical linear theories.

We have confirmed the unique and significant modeling power when adopting both absement and generalized momentum, the time integral of strain and stress in the mem-springs and mem-dashpots for modeling elastic damage strain and ratcheting strain, respectively. These choices of state variables for the nonlinear state-space representation enable governing one-to-one mappings to be preserved after introducing switching behaviors under a hybrid dynamical system viewpoint. One-to-one mappings are probably among the most desired portraits of complex time-dependent and history/path-dependent and fundamentally nonlinear dynamic systems that the mem-models contribute, even with the necessity of adopting other state variables being acknowledged.

Since the classical Preisach model for hysteresis is rigorous, showing that two forms of time-invariant memcapacitive system models are a subset provides a rigorous foundation for the latter. For this subset, using the mem-models reduces computational demand and also enables a physical interpretation. Nevertheless, the nonlocal memory in Preisach model is still demanding computationally. More state variables must be introduced and/or algebraic variables are needed for capturing nonlocal memory when higher-order responses of the Preisach model are anticipated.

REFERENCES

Beck JL, Jayakumar P (1996) Class of masing models for plastic hysteresis in structures. In: Proceedings 14th ASCE Structures Congress, Chicago, IL

Bennett KC, Zecevic M, Luscher DJ, Lebensohn RA (2020) A thermo-elastoplastic self-consistent homogenization method for inter-granular plasticity with application to thermal ratcheting of tatb. Adv Model and Simul in Eng Sci 7(3)

Biolek D, Biolek Z, Biolkova V (2016) Memristors and other higher-order elements in generalized through-across domain. In: Proceedings of the 2016 IEEE International Conference on Electronics, Circuits and Systems (ICECS), Monte Caro, Monaco

Chaboche JL (1987) Continuum damage mechanics: Present state and future trends. Nuclear Engineering and Design 105:19–33

Chua LO (1971) Memrister - the missing circuit element. IEEE Transactions on Circuit Theory CT-18(5):507–519

Chua LO (2003) Nonlinear circuit foundations for nanodevices, part i: The four-element torus. In: Proceedings of the IEEE, vol 91

Chua LO, Kang SM (1976) Memristive devices and systems. In: Proceedings of the IEEE, vol 64, pp 209–223

Di Ventra M, Pershin YV, Chua LO (2009) Circuit elements with memory: Memristors, memcapacitors, and meminductors. In: Proceedings of IEEE, vol 97, pp 1717–1724

Fan WRS (1968) The damping properties and the earthquake response spectrum of steel frames. PhD thesis, University of Michigan, Ann Arbor, MI

Goldfarb M, Celanovic N (1996) Modeling piezoelectric stack actuators for control of micromanipulation. In: Proceedings of the 1996 IEEE International Conference on Robotics and Automation, Minneapolis, MN

Gorbet RB, Morris KA, Wang DWL (1998) Learning, control, and hybrid systems, Springer-Verlag, New York, chap Control of hysteretic systems: a statespace approach, pp 432–451

Gurtin ME, Francis EC (1981) Simple rate-independence model for damage. J Spacecraft 18(3):285–286, engineering Notes

Houlsby GT, Puzrin AM (2007) Principles of Hyperplasticity: An Approach to Plasticity Theory Based on Thermodynamic Principles. Springerr

Houslby GT, Abadie CN, Beuckelaers WJAP, Byrne BW (2017) A model for nonlinear hysteretic and ratcheting behaviour. International Journal of Solids and Structures 120:67–80

Iwan WD (1966) A distributed-element model for hysteresis and its steady-state dynamic response. ASME Journal of Applied Mechanics 33(4):893–900

Iwan WD (1967) On a class of models for the yielding behavior of continuous and composite systems. ASME J Appl Mech 34(3):612–617

Jayakumar P (1987) Modeling and identification in structural dynamics. PhD thesis, California Institute of Technology, Pasadena, CA

Jayakumar P, Beck JL (1988) System identification using nonlinear structural models. In: Nake HG, Yao JTP (eds) Structural Safety Evaluation Based on System Identification Approaches, Friedr. Vieweg & Sohn Braunschweig/Wiesbaden, Vieweg International Scientific Book Series, vol Proceedings of the Workshop at Lambrecht/Pfalz, pp 82–102

Jeltsema D (2012) Memory elements: A paradigm shift in lagrangian modeling of electrical circuits. In: Proc. MathMod Conference, Vienna

Jeltsema D, Scherpen JMA (2009) Multidomain modeling of nonlinear networks and systems: Energy- and power-based perspectives. IEEE Control Systems Magazine pp 28–59

Kachanov LM (1986) Introduction to Continuum Damage Mechanics. Mechanics of Elastic Stability, Martinus Nijhoff Publishers, Dordrercht

Kalman RE (1967) Algebraic aspects of the theory of dynamical systems. In: Hale J, LaSalle J (eds) Differential Equations and Dynamical Systems, Academic Press, New York and London, pp 133 – 146

Krasnosel'skii MA, Pokrovskii AV (1989) Systems with Hysteresis. Springer-Verlag

Lemaitre J (1985) A continuous damage mechanics model for ductile fracture. Journal of Engineering Materials and Technology 107:83–89

Lemaitre J (1996) A Course on Damage Mechanics, 2nd edn. Springer-Verlag

Lemaitre J, Chaboche JL (1990) Mechanics of Solid Materials. Cambridge University Press

Lubarda VA, Sumarac D, Krajcinovic D (1993) Preisach model and hysteretic behaviour of ductile materials. Eur J Mech A/Solids 12(4):445–470

Masing G (1926) Eigenspannungen und verfestigung beim messing. In: Proceedings of the 2nd International Congress for Applied Mechanics, Zurich, Switzerland, pp 332–335, in German

Mayergoyz ID (2003) Mathematical Models of Hysteresis and Their Applications. Elsevier Series in Electromagnetism, Elsevier

McDowell DL, Miller MP, Brooks DC (1994) A unified creep-plasticity theory for solder alloys. In: Schroeder S, Mitchell M (eds) Fatigue of Electronic Materials, ASTM International, West Conshohocken, PA, pp 42–59

Moosbrugger JC, McDowell DL (1990) A rate-dependent bounding surface model with a generalized image point for cyclic nonproportional viscoplasticity. Journal of the Mechanics and Physics of Solids 38(5):627–656

Morris KA (2011) What is hysteresis? Applied Mechanics Review 64(5):14 pages

Oster GF, Auslander DM (1973) The memristor: A new bond graph element. ASME Journal of Dynamic Systems, Measurement, and Control 94(3):249–252

Padthe AK, Drincic B, Oh J, Rizos DD, Fassois SD, Bernstein DS (2008) Duhem modeling for friction-induced hysteresis. IEEE Control Systems Magazine 28(5):90–107

Paul SK (2019) A critical review of experimental aspects in ratcheting fatigue: microstructure to specimen to component. Journal of Materials Research and Technology 8(5):4894–4914

Pei JS (2018) Mem-spring models combined with hybrid dynamical system approach to represent material behavior. ASCE Journal of Engineering Mechanics 144(12)

Pei JS, Beck JL (2020) Understanding nonlocal memory in extended masing models for hysteresis through model equivalency and numerical investigation. Nonlinear Dynamics Under review for publication

Pei JS, Wright JP, Todd MD, Masri SF, Gay-Balmaz F (2015) Understanding memristors and memcapacitors for

engineering mechanical applications. Nonlinear Dynamics 80(1):457–489
Pei JS, Gay-Balmaz F, Wright JP, Todd MD, Masri SF (2017) Dual input-output pairs for modeling hysteresis inspired by mem-models. Nonlinear Dynamics 88(4):2435–2455
Pei JS, Wright JP, Gay-Balmaz F, Beck JL, Todd MD (2018) On choosing state variables for piecewise-smooth dynamical system simulations. Nonlinear Dynamics
Pei JS, Carboni B, Lacarbonara W (2020a) Mem-models as building blocks for simulation and identification of hysteretic systems. Nonlinear Dynamics
Pei JS, Quadrelli MB, Wright JP (2020b) Mem-models and state event location algorithm for a prototypical aerospace system. Nonlinear Dynamics
Preisach F (1935) About the magnetic aftereffect. Magazine for Physics 94(5-6):277–302
Pyke R (1979) Nonlinear soil models for irregular cyclic loadings. Journal of the Geotechnical Engineering Division, ASCE 105:715–726
Roylance D (2001) Engineering viscoelasticity. *https://ocw.mit.edu/courses/materials-science-and-engineering/3-11-mechanics-of-materials-fall-1999/modules/MIT3_11F99_visco.pdf*
Royston TJ (2008) Leveraging the equivalence of hysteresis models from different fields for analysis and numerical simulation of jointed structures. ASME Journal of Computational and Nonlinear Dynamics 3:031,006–1 – 031,006–8
Segalman DJ, Starr MJ (2004) Relationships among certain joints constitutive models. Report SAND2004-4321, Sandia National Laboratories
Segalman DJ, Starr MJ (2008) Inversion of Masing models via continuous Iwan systems. International Journal of Non-Linear Mechanics 43:74–80
Song C, Brandon JA, Featherston CA (2001) Distributed-element preisach model for hysteresis of shape memory alloys. Proc Instn Mech Engrs 215:673–682
Strukov DB, Snider GS, Stewart DR, Williams RS (2008) The missing memristor found. Nature 453:80–83
Visintin A (1994) Differential Models of Hysteresis. Springer
Wagg JD, Pei JS (2020) Modeling helical fluid inerter system with invariant mem-models. Journal of Structural Control and Health Monitoring
Willems JC (1972) Dissipative dynamical systems part i: General theory. Arch Rational Mech Anal 45:321–351

ACKNOWLEDGEMENTS

Professor Jin-Song Pei acknowledges the University of Oklahoma for the teaching release offered in the fall of 2019 and the hospitality of Professor Raimondo Betti at Columbia University. Dr. Marco Quadrelli's research was carried out at the Jet Propulsion Laboratory, California Institute of Technology, under a contract with the NASA Aeronautics and Space Administration. In particular, Jin-Song Pei and Marco B. Quadrelli acknowledge the Oklahoma NASA EPSCoR for the Faculty Research Initiation Fellowship. Government sponsorship acknowledged.

ETHICALI STATEMENT

The authors declare that they have no conflict of interest.

A Appendix

A.1 Some Basic Energy Relations

The following discussion is for a flow-controlled system, starting with an imposed constant strain rate, followed by strain removal at the same rate:

$$\text{imposed strain, } t \in [0, t_0]\text{: } \varepsilon(t) = k_\varepsilon t \tag{96}$$

$$\text{strain removal, } t \in [t_0, 2t_0]\text{: } \varepsilon(t) = \underbrace{k_\varepsilon t_0}_{\varepsilon_0} - k_\varepsilon(t - t_0), \tag{97}$$

where k_ε is the strain rate, and $t = t_0$ is the time when strain removal starts.

The energy per unit volume of material, U, is the area under the corresponding stress-strain curve:

$$U = \int_0^{\varepsilon_0} \sigma_l d\varepsilon_l + \int_{\varepsilon_0}^0 \sigma_u d\varepsilon_u \tag{98}$$

where l and u are for loading and unloading, respectively.

1. Piece-wise defined nonlinear spring, i.e., $\sigma = f_i(\varepsilon)$

$$\begin{aligned} U(t) &= \int_0^{t_0} f_l\left(k_\varepsilon \tau\right) k_\varepsilon d\tau + \int_{t_0}^{2t_0} f_u\left(-k_\varepsilon \tau + 2\varepsilon_0\right)\left(-k_\varepsilon\right) d\tau \\ &= k_\varepsilon \int_0^{t_0} \left[f_l(k_\varepsilon \tau) - f_u(-k_\varepsilon \tau + \varepsilon_0)\right] d\tau, \end{aligned} \tag{99}$$

where τ is the dummy index for time t. Notable examples including Ramberg-Osgood models and Bouc-Wen models.

2. Viscoelastic material, i.e., $\sigma = f(\dot{\varepsilon})$

$$\begin{aligned} U(t) &= \int_0^{t_0} f(k_\varepsilon) k_\varepsilon d\tau + \int_{t_0}^{2t_0} f(-k_\varepsilon)(-k_\varepsilon) d\tau \\ &= k_\varepsilon \int_0^{t_0} \left[f(k_\varepsilon) - f(-k_\varepsilon)\right] d\tau \end{aligned} \tag{100}$$

3. Mechanical memcapacitor, i.e., $\sigma = f(a)\varepsilon$

$$\begin{aligned} U(t) &= \int_0^{t_0} f\left(\frac{k_\varepsilon}{2}\tau^2\right) k_\varepsilon d\tau \\ &\quad + \int_{t_0}^{2t_0} f\left(-\frac{k_\varepsilon}{2}\tau^2 + 2\varepsilon_0 \tau - \varepsilon_o t_0\right)\left(-k_\varepsilon\right) d\tau \\ &= k_\varepsilon \int_0^{t_0} \left[f\left(\frac{k_\varepsilon}{2}\tau^2\right) - f\left(-\frac{k_\varepsilon}{2}\tau^2 + \varepsilon_0 \tau + \frac{1}{2}\varepsilon_0 t_0\right)\right] d\tau \end{aligned} \tag{101}$$

A.2 Mem-Spring Calibrated to Linear Viscoelastic Models

Mem-springs, being fundamentally nonlinear, cannot be expected to behave like linear models. Consequently, it was hard to avoid some initial mistakes in the following effort, the goal being to calibrate a mem-spring to make it respond the same as a linear model under a specific input (but only for a specific duration of time). Then, we change the input to reveal their differences.

Element models are tried before system models for the mem-spring. First of all, memcapacitor models are good for both $\varepsilon(t) = k_\varepsilon t$ and $\sigma(t) = k_\sigma t$ to produce a maybe-valid stress-strain curve for viscoelastic material. Next, to what extent a memcapacitor model can be calibrated to a linear model demands attention.

(i) Maxwell model: Only good for $\varepsilon(t) = k_\varepsilon t$ (i.e., $a = \frac{1}{2}k_\varepsilon t^2$) to produce a typical stress-strain curve for viscoelastic material as

$$\sigma(t) = k_\varepsilon \eta \left[1 - e^{-\frac{E}{\eta}t}\right] \tag{102}$$

$$p(t) = k_\varepsilon \eta t + \frac{k_\varepsilon \eta^2}{E} e^{-\frac{E}{\eta}t} - \frac{k_\varepsilon \eta^2}{E} \tag{103}$$

We can calibrate a memcapacitor (i.e., an element) $\sigma(t) = S(a(t))\varepsilon(t)$, or equivalently, $p(t) = G(a(t))$ as follows:

$$p = G(a) = k_\varepsilon \eta \sqrt{\frac{2a}{k_\varepsilon}} + \frac{k_\varepsilon \eta^2}{E} e^{-\frac{E}{\eta}\sqrt{\frac{2a}{k_\varepsilon}}} - \frac{k_\varepsilon \eta^2}{E} \tag{104}$$

with the understanding that Maxwell and mem-spring models would only respond the same under any specific value of k_ε in $\varepsilon(t) = k_\varepsilon t$. The corresponding one-to-one mapping $S(a) = \frac{dG}{da}$ is as follow:

$$S(a) = \frac{\eta \left[1 - e^{-\frac{E}{\eta}\sqrt{\frac{2a}{k_\varepsilon}}}\right]}{\sqrt{\frac{2a}{k_\varepsilon}}} \tag{105}$$

Note that an attempt of continuing with the calibration using the unloading behavior of the same Maxwell model failed. Details are given as follow when $a = -\frac{1}{2}k_\varepsilon (t - t_0)^2 + 2a_0$ for $t \in [t_0, 2t_0]$:

$$\sigma(t) = -k_\varepsilon \eta - k_\varepsilon \eta e^{-\frac{E}{\eta}t} + 2k_\varepsilon \eta e^{-\frac{E}{\eta}(t-t_0)} \tag{106}$$

$$p(t) = -k_\varepsilon \eta t + \frac{k_\varepsilon \eta^2}{E} e^{-\frac{E}{\eta}t} - \frac{2k_\varepsilon \eta^2}{E} e^{-\frac{E}{\eta}(t-t_0)} + p_0 \tag{107}$$

It would not be possible to use the same memcapacitor model for this unloading behavior.

(ii) Kelvin model: Only good for $\sigma(t) = k_\sigma t$ (i.e., $p = \frac{1}{2}k_\sigma t^2$) to produce a typical stress-strain curve for viscoelastic material as

$$\varepsilon(t) = \frac{k_\sigma}{E} t - \frac{k_\sigma \eta}{E^2}\left[1 - e^{-\frac{E}{\eta}t}\right] \tag{108}$$

$$a(t) = \frac{k_\sigma}{2E} t^2 - \frac{k_\sigma \eta}{E^2} t + \frac{k_\sigma \eta^2}{E^3}\left[1 - e^{-\frac{E}{\eta}t}\right] \tag{109}$$

We can calibrate a mem-spring (i.e., an element) $\varepsilon(t) = C(p(t))\sigma(t)$, or equivalently, $a(t) = F(p(t))$ as follows:

$$a = F(p) = \frac{p}{E} - \frac{k_\sigma \eta}{E^2}\sqrt{\frac{2p}{k_\sigma}} + \frac{k_\sigma \eta^2}{E^3}\left[1 - e^{-\frac{E}{\eta}\sqrt{\frac{2p}{k_\sigma}}}\right] \tag{110}$$

with the understanding that Kelvin and mem-spring models would only respond the same under any specific value of k_σ in $\sigma(t) = k_\sigma t$. The corresponding one-to-one mapping $C(p) = \frac{dF}{dp}$ is as follow:

$$C(p) = \frac{1}{E} - \frac{\frac{\eta}{E^2}\left[1 - e^{-\frac{E}{\eta}\sqrt{\frac{2p}{k_\sigma}}}\right]}{\sqrt{\frac{2p}{k_\sigma}}} \tag{111}$$

The rest challenge remains as for calibrating using the Maxwell model.

See Figs. 22 and 23 for two numerical examples.

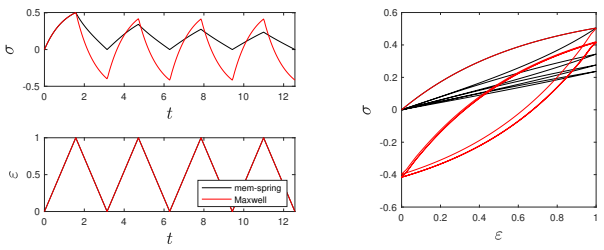

Fig. 22: One example of "calibrating" a particular Maxwell model with $E = 1$, $\eta = 1$ and $k_\varepsilon = \frac{2}{\pi}$

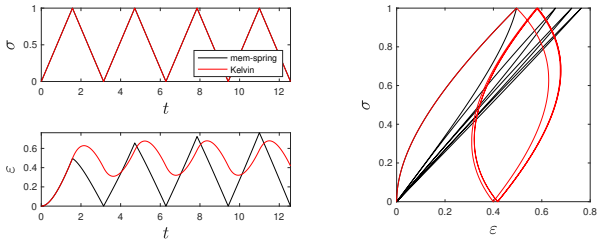

Fig. 23: One example of "calibrating" a particular Kelvin model with $E = 1$, $\eta = 1$ and $k_\sigma = \frac{2}{\pi}$